HHS Public Access

Author manuscript

Cell. Author manuscript; available in PMC 2025 January 04.

Published in final edited form as:

Cell. 2024 January 04; 187(1): 44–61.e17. doi:10.1016/j.cell.2023.11.027.

Sensory Neurons Promote Immune Homeostasis in the Lung

Masato Tamari[1,2,3,4,5,6], **Kate L. Del Bel**[7], **Aaron M. Ver Heul**[8], **Lydia Zamidar**[1,2,3,4], **Keisuke Orimo**[6], **Masato Hoshi**[9,10], **Anna M. Trier**[11], **Hiroshi Yano**[12,13,14], **Ting-Lin Yang**[11], **Catherine M. Biggs**[7], **Kenichiro Motomura**[6], **Rintaro Shibuya**[1,2,3,4], **Chuyue D. Yu**[15,16], **Zili Xie**[1,2,4], **Hisato Iriki**[1,2,3,4], **Zhen Wang**[1,2,3,4], **Kelsey Auyeung**[1,2,3,4], **Gargi Damle**[17,18], **Deniz Demircioglu**[17,18], **Jill K. Gregory**[19], **Dan Hasson**[17,18,20,21], **Jinye Dai**[22,23], **Rui B. Chang**[15,16,24], **Hideaki Morita**[6,25], **Kenji Matsumoto**[6], **Sanjay Jain**[9,10], **Steven Van Dyken**[9], **Joshua D. Milner**[26], **Dusan Bogunovic**[3,17,20,27,28,29,30], **Hongzhen Hu**[1,2,4], **David Artis**[12,13,14,24,31], **Stuart E. Turvey**[7], **Brian S. Kim**[1,2,3,4,24,32,*]

[1]Kimberly and Eric J. Waldman Department of Dermatology, Icahn School of Medicine at Mount Sinai, New York, NY 10029, USA

[2]Mark Lebwohl Center for Neuroinflammation and Sensation, Icahn School of Medicine at Mount Sinai, New York, NY 10029, USA

[3]Marc and Jennifer Lipschultz Precision Immunology Institute, Icahn School of Medicine at Mount Sinai, New York, NY, 10029, USA

[4]Friedman Brain Institute, Icahn School of Medicine at Mount Sinai, New York, NY, 10029, USA

[5]Department of Pediatrics, Jikei University School of Medicine, Minato-ku, Tokyo, 1058471, Japan

[6]Department of Allergy and Clinical Immunology, National Research Institute for Child Health and Development, Setagaya-ku,Tokyo, 1578535, Japan

[7]Department of Pediatrics, British Columbia Children's Hospital, University of British Columbia, Vancouver, British Columbia, BC V5Z 4H4, Canada

[*]Correspondence: Brian S. Kim, MD, MTR, Icahn School of Medicine at Mount Sinai, 1425 Madison Avenue, New York, NY, 10029. itchdoctor@mountsinai.org.

AUTHOR CONTRIBUTIONS

Conceptualization, M.T. and B.S.K.; Methodology, M.T., K.L.D.B., A.M.V.H., L.Z., K.O., M.H., A.M.T., H.Y., C.D.Y., Z.X., G.D., D.D., D.H., R.B.C., H.M., K.M., S.J., H.H. S.E.T., and B.S.K.; Validation, M.T. and A.M.V.H.; Formal Analysis, M.T, A.M.V.H., G.D., D.D., and D.H.; Investigation, M.T., K.L.D.V., A.M.V.H., K.O., H.Y., T.L.Y., C.M.B., G.D., D.D., and D.H.; Resources, M.H. H.Y., G.D., D.D., J.K.G., D.H., J.D., R.B.C., H.M., K.M. S.J. S.V.D., J.M., D.B., H.H., D.A., S.E.T., and B.S.K.; Writing – Original Draft, M.T.; Writing – Review & Editing, All authors; Supervision, B.S.K., Funding Acquisition, B.S.K.

DECLARATION OF INTERESTS

B.S.K. is founder of Klirna Biotech; he has served as a consultant for 23andMe, ABRAX Japan, AbbVie, Almirall, Amgen, Arcutis Biotherapeutics, Arena Pharmaceuticals, argenx, AstraZeneca, Boehringer Ingelheim, Bristol-Myers Squibb, Cara Therapeutics, Clexio Biosciences, Eli Lilly and Company, Escient Pharmaceuticals, Evommune, Galderma, Genentech, GlaxoSmithKline, Granular Therapeutics, Incyte Corporation, Innovaderm Research, Janssen, Kiniksa, LEO Pharma, Maruho, Novartis, Pfizer, Recens Medical, Regeneron Pharmaceuticals, Sanofi, Septerna, Triveni Bio, Vial, WebMD; he has stock in ABRAX Japan, KliRNA Biotech, Locus Biosciences, and Recens Medical; he holds a patent for the use of JAK1 inhibitors for chronic pruritus; he has a patent pending for the use of JAK inhibitors for interstitial cystitis. D.A. has contributed to scientific advisory boards at Pfizer, Takeda, FARE, and the KRF. D.B. is the founder of Lab11 Therapeutics. All other authors declare that they have no relevant conflicts of interests.

[8]Division of Allergy and Immunology, Department of Medicine, Washington University School of Medicine, St. Louis, MO, 63130, USA

[9]Department of Pathology and Immunology, Washington University School of Medicine, St. Louis, MO, 63130, USA

[10]Division of Nephrology, Department of Medicine, Washington University School of Medicine, St. Louis, MO, 63130, USA

[11]Division of Dermatology, Department of Medicine, Washington University School of Medicine, St. Louis, MO, 63110, USA

[12]Jill Roberts Institute for Research in Inflammatory Bowel Disease, Weill Cornell Medicine, Cornell University, New York, NY, 10021, USA

[13]Joan and Sanford I. Weill Department of Medicine, Division of Gastroenterology and Hepatology, Weill Cornell Medicine, Cornell University, New York, NY, 10021, USA

[14]Department of Microbiology and Immunology, Weill Cornell Medicine, Cornell University, New York, NY, 10021, USA

[15]Department of Neuroscience, Yale University School of Medicine, New Haven, CT, 06510, USA

[16]Department of Cellular and Molecular Physiology, Yale University School of Medicine, New Haven, CT, 06510, USA

[17]Tisch Cancer Institute Bioinformatics for Next Generation Sequencing (BiNGS) Core, Icahn School of Medicine at Mount Sinai, New York, NY, 10029, USA

[18]Skin Biology and Disease Resource-based Center, Icahn School of Medicine at Mount Sinai, New York, NY, 10029, USA

[19]Digital and Technology Partners, Icahn School of Medicine at Mount Sinai, New York, NY 10029, USA

[20]Department of Oncological Sciences, Icahn School of Medicine at Mount Sinai, New York, NY, 10029, USA

[21]Graduate School of Biomedical Sciences, Icahn School of Medicine at Mount Sinai, New York, NY, 10029, USA

[22]Department of Pharmacological Science, Icahn School of Medicine at Mount Sinai, New York, NY, 10029, USA

[23]Department of Neuroscience, Icahn School of Medicine at Mount Sinai, New York, NY, 10029, USA

[24]Allen Discovery Center for Neuroimmune Interactions, New York, NY 10029, USA

[25]Allergy Center, National Center for Child Health and Development, Setagaya-ku, Tokyo, 1578535, Japan

[26]Division of Allergy, Immunology, and Rheumatology, Department of Pediatrics, Columbia University Vagelos College of Physicians and Surgeons, New York, NY, 10032, USA

[27]Department of Microbiology, Icahn School of Medicine at Mount Sinai, New York, NY, 10029, USA

[28]Center for Inborn Errors of Immunity, Icahn School of Medicine at Mount Sinai, New York, NY, 10029, USA

[29]Mindich Child Health and Development Institute, Icahn School of Medicine at Mount Sinai, New York, NY, 10029, USA

[30]Department of Pediatrics, Icahn School of Medicine at Mount Sinai, New York, NY, 10029, USA

[31]Friedman Center for Nutrition and Inflammation, Weill Cornell Medicine, Cornell University, New York, NY, 10021, USA

[32]Lead contact

SUMMARY

Cytokines employ downstream Janus kinases (JAKs) to promote chronic inflammatory diseases. JAK1-dependent type 2 cytokines drive allergic inflammation, and patients with *JAK1* gain-of-function (GOF) variants develop atopic dermatitis (AD) and asthma. To explore tissue-specific functions, we inserted a human *JAK1* GOF variant (*JAK1*^{GOF}) into mice and observed the development of spontaneous AD-like skin disease, but unexpected resistance to lung inflammation when *JAK1*^{GOF} expression was restricted to the stroma. We identified a previously unrecognized role for JAK1 in vagal sensory neurons in suppressing airway inflammation. Additionally, expression of *Calcb*/CGRPβ, was dependent on JAK1 in vagal sensory neurons, and CGRPβ suppressed group 2 innate lymphoid cell function and allergic airway inflammation. Our findings reveal evolutionarily conserved but distinct functions of JAK1 in sensory neurons across tissues. This biology raises the possibility that therapeutic JAK inhibitors may be further optimized for tissue-specific efficacy to enhance precision medicine in the future.

In Brief

Janus kinase 1 signaling exerts distinct effects across cell types and tissues, with JAK1 signaling in vagal sensory neurons promoting anti-inflammatory responses in the lung.

Graphical Abstract

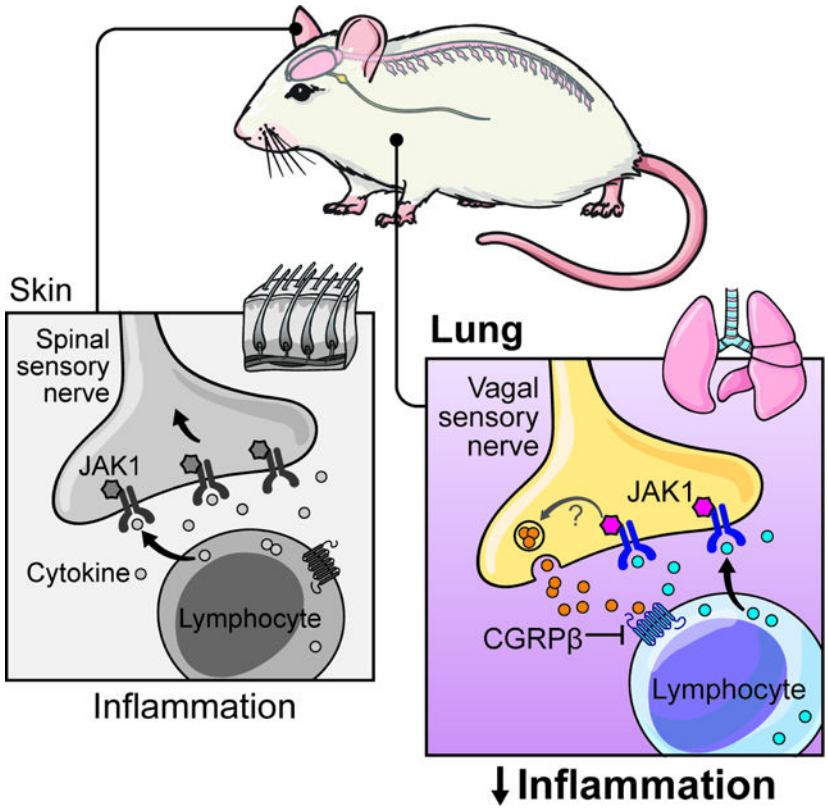

Keywords

AAV; afferent nerves; allergic lung inflammation; atopic disorders; CGRP; ILC2; JAK1; neuropeptide; sensory neurons; vagus nerve

INTRODUCTION

Cytokine receptors commonly employ the Janus kinase (JAK)-signal transducers and activators of transcription (STAT) pathway to influence effector cell programs. Indeed, JAK inhibition has revolutionized the treatment of a number of inflammatory, myeloproliferative, and even infectious disorders.[1] Interest in the therapeutic potential of JAK inhibitors across the spectrum of allergic disorders is rapidly growing. In the past year, two JAK1-selective inhibitors were approved by the FDA for treatment of atopic dermatitis (AD), and several clinical trials for asthma treatment are underway.[2–6] However, little is known about the pathophysiologic consequences of JAK inhibition. Indeed, the precise mechanisms underlying major adverse events of JAK inhibitor treatment, including cardiovascular events (MACE), cancer, and opportunistic infections, remain poorly defined.[7] Thus, understanding the tissue-specific role of JAK signaling across organs can simultaneously inform understanding of biology but also foreshadow how JAK inhibitors may be used across the evolving medical landscape.

Type 2 cytokines critically rely on downstream JAK1 signaling to promote allergic inflammation.[8] However, much of what we know about JAK inhibition has derived from

our understanding of cytokine signaling within the hematopoietic compartment.[9] Although, in immune cells, JAK1 phosphorylation drives a proinflammatory effector program,[1] The role of JAK1 signaling within stromal cells (e.g., epithelial cells, fibroblasts, etc.) is just beginning to be uncovered. For example, sensory neuron-intrinsic JAK1 was found to play an unexpected role in promoting itch sensation, a difficult-to-treat component of AD pathology.[10] Thus, probing the tissue- and cell-specific effects of JAK1 signaling is critical to understanding the molecular and cellular basis of allergic disease pathogenesis and treatment.

Patients with germline *JAK1* gain-of-function (GOF) variants (*JAK1*^{GOF}) develop atopic disorders such as AD and asthma, as well as eosinophilia.[11,12] We sought to utilize a pathogenic human *JAK1* GOF variant to probe the precise tissue-intrinsic mechanisms by which JAK1 signaling orchestrates various allergic pathologies. To do this, we generated a mouse line in which the endogenous murine *Jak1* gene was replaced with a human *JAK1* GOF mutation (*JAK1*^{GOF} mice) that was reported in 2017.[11] Although these mice exhibited spontaneous AD-like inflammation, as observed in patients, no lung pathology was evident at steady state. However, global *JAK1*^{GOF} mice exhibited enhanced allergic lung inflammation in response to the classic aeroallergen *Alternaria alternata*. Strikingly, restriction of *JAK1*^{GOF} expression to the stroma rendered mice resistant to allergic lung inflammation. Given recent reports that sensory neurons can suppress lung inflammation,[13–18] we hypothesized that sensory neurons mediate a key regulatory circuit through JAK1 signaling.

Indeed, we found that chemical denervation of lung tissue as well as conditional deletion of endogenous murine *Jak1* in sensory neurons aggravated allergic lung inflammation. We screened various neuropeptides associated with neuroinflammation and discovered that expression of *Jak1* is required for proper expression of *Calcb*, which encodes the neuropeptide calcitonin gene-related peptide β (CGRPβ), within the vagal ganglia (VG). Additionally, we found that CGRPβ suppresses pathogenic group 2 innate lymphoid cell (ILC2) responses and allergic lung inflammation. Finally, retrograde viral delivery of *JAK1*^{GOF} to the lung resulted in selective uptake into the VG and suppression of allergic lung inflammation. Similarly, conditional insertion of *JAK1*^{GOF} into sensory neurons also promoted immune homeostasis in the lung.

Collectively, our study highlights that while JAK1 signaling promotes skin inflammation and is a major therapeutic target for AD and itch, sensory neuron-intrinsic signaling of JAK1 serves an immunoregulatory role in the lung. We reveal a previously unrecognized role for neuronal JAK1 in regulating neuropeptide expression and neuroinflammation. These findings underscore the importance of understanding tissue-specific JAK signaling across mammalian systems and the potential utility of JAK inhibitors across the disease spectrum.

RESULTS

Germline human *JAK1* GOF promotes spontaneous allergic inflammation in the skin, but not in the lung

The first patients harboring a germline *JAK1* GOF mutation were identified in 2017 as an alanine-to-aspartate substitution at position 634 (A634D) within the inhibitory pseudokinase domain of the JAK1 protein. These patients exhibited a number of allergic pathologies, including AD, asthma, and profound eosinophilia (Figure 1A).[11] However, the severity of the patients' AD and asthma were not reported in the original study. Thus, we examined the clinical characteristics of two patients when they originally presented with AD and asthma symptoms in more detail. Indeed, both patients with *JAK1* GOF mutations presented with AD markedly earlier in life than with asthma (Figure 1B). Further, the overall relative severity of their AD (Figures 1C–E) was generally worse than the severity of their asthma as determined by quantitative and validated metrics such as Eczema Area and Severity Index (EASI) scores (Figure 1E), forced expiratory volume (FEV1) (Figure 1F), and forced vital capacity (FVC) (Figure 1G) measurements. These findings suggest that activation of JAK1 across multiple tissues results in differential tissue-specific outcomes.

To examine how JAK1 confers unique effects across tissues, we generated mice in which the endogenous murine *Jak1* gene was replaced with the mutant human *JAK1* GOF variant (A634D) (Figure 1H). Strikingly, soon after birth, heterozygous *JAK1*^{GOF} mice display spontaneous AD-like dermatitis with increased skin thickness compared to the skin of wild-type (WT) control mice (Figures 1I–J). Histologically, the *JAK1*^{GOF} mice exhibited hyperkeratosis, epidermal hyperplasia, and dermal inflammatory immune cell infiltrate that were not observed in control mice (Figure 1K). Further, the *JAK1*^{GOF} mice demonstrated a higher frequency of immune cell populations commonly associated with allergic inflammation, including total CD45^{+} immune cells (Figures 1L), CD4^{+} T cells (Figures 1M), ILC2s (Figures 1N), and eosinophils (Figures 1O) in the skin-draining lymph nodes compared to control mice at steady state. Taken together, these findings demonstrate that even one germline copy of the human *JAK1* GOF allele is sufficient to drive AD-like pathology in mice, recapitulating the human skin phenotype.

Surprisingly, in contrast to the skin, the lungs of *JAK1*^{GOF} mice did not display spontaneous inflammatory pathology when compared to those from age-matched WT control counterparts. In both *JAK1*^{GOF} and control mice, assessment of airway remodeling and inflammatory infiltrate by hematoxylin and eosin (H&E) staining revealed no histopathologic evidence of lung inflammation (Figure 1P), and periodic acid-Schiff (PAS) staining revealed no evidence of goblet cell hyperplasia and mucus production (Figure 1Q). Further, the extent of CD45^{+} immune cell (Figures 1R and S1), CD4^{+} T cell (Figures 1S and S1), ILC2 (Figures 1T and S1), and eosinophil (Figures 1U and S1) enrichment was comparable if not reduced in the *JAK1*^{GOF} mice compared to control mice. Collectively, these findings provoke the hypothesis that the lung harbors resistance to JAK1-mediated inflammation that is not observed in the skin.

Stromal *JAK1*^{GOF} suppresses allergen-induced lung inflammation

We next examined whether challenging the airway with an allergen might provoke an enhanced inflammatory response not observed at steady state. To test this hypothesis, we treated both *JAK1*^{GOF} and control mice intranasally with the asthma-associated fungal allergen *Alternaria alternata* (Figure 2A). In this well-established model of allergic lung inflammation, ILC2s promote eosinophil responses and allergic lung pathology.[19–22] Indeed, histopathologic analysis revealed enhanced lung pathology in *JAK1*^{GOF} mice compared to controls as demonstrated by increased airway remodeling, inflammatory infiltrate, goblet cell hyperplasia, and mucus production upon provocation by the allergen (Figures 2B–C). Further, we found that *Alternaria alternata*-treated *JAK1*^{GOF} mice exhibit significantly elevated frequencies of ILC2s in their lungs compared to control mice (Figure 2D); however, we did not observe a difference in eosinophil frequency (Figure 2E). Taken together, these findings indicate that although global activation of JAK1 does not result in spontaneous allergic inflammation in the lung, provocation with an allergen renders *JAK1*^{GOF} mice more susceptible to some features of allergic lung pathology.

Given the resistance to JAK1-mediated inflammation observed in the lung at steady state, we hypothesized that JAK1 activation within the lung stroma may confer tissue-specific resistance even upon allergen challenge. To test this hypothesis, we generated bone marrow (BM) chimeric mice in which we reconstituted both control and *JAK1*^{GOF} mice with WT BM (WT→WT and WT→*JAK1*^{GOF}) (Figures 2F–G). Upon airway challenge with *Alternaria alternata* (Figure 2H), WT→*JAK1*^{GOF} mice exhibited markedly reduced lung pathology as evidenced by reduced peribronchial and perivascular inflammatory infiltrates (Figure 2I), goblet cell hyperplasia, and mucous production (Figure 2J) when compared to control WT→WT mice. Further, the frequencies of ILC2s (Figure 2K) and eosinophils (Figure 2L) were significantly reduced in WT→*JAK1*^{GOF} mice compared to control WT→WT mice. Strikingly, KEGG pathway overrepresentation analysis of RNA-seq data obtained from lung tissue showed that expression of asthma- and inflammation-associated pathways were significantly suppressed in WT→*JAK1*^{GOF} mice compared to control WT→WT mice (Figure 2M). While it is well-appreciated that *JAK1*^{GOF} activates lymphocytes, these unanticipated findings indicate that stromal expression of *JAK1*^{GOF} confers resistance to lung inflammation.

Sensory neurons suppress allergic lung inflammation

Recent studies demonstrated that neuropeptides can restrain ILC2 responses and lung inflammation.[16,18] Thus, we hypothesized that sensory neurons in the lung may act to suppress inflammation. In contrast to the skin, which is almost entirely innervated by sensory neurons arising from the dorsal root ganglia (DRG), the lung is primarily innervated by sensory afferents that arise from the VG, with minor innervation from the DRG[23] (Figure 3A). The majority of sensory neurons from the DRG express canonical nociceptive markers such as TRPV1 and $Na_v1.8$.[24–26] Sensory neurons in the vagus nerve exhibit expression of nociceptive ion channels comparable to that observed in DRG-derived neurons,[27] as evidenced in our reanalysis of recently published single cell RNA-seq (scRNA-seq) datasets from vagal afferents[28] (Figures 3B–C). To visualize the extent of TRPV1 and $Na_v1.8$ expression within the VG and DRG, we generated reporter mice by crossing *Trpv1*^{Cre} and

Scn10a^{Cre}, respectively, to *Rosa26*$^{STOPflox\text{-}tdTomato}$ mice. Imaging of these reporter mice revealed widespread expression of both TRPV1 and $Na_V1.8$ in both ganglia (Figures 3D–E). These findings suggested that sensory neurons within the VG can be chemically, genetically, and virally targeted.

TRPV1-expressing neurons can be chemically denervated by treatment with resiniferatoxin (RTX), an ultrapotent TRPV1 agonist.[29,30] The majority of lung sensory innervation arises from vagal afferents while only a small proportion originates from DRG-derived spinal sensory neurons (i.e., spinal visceral afferents).[23] Therefore, we first examined whether $TRPV1^+$ neurons, including vagal and spinal sensory neurons, contribute to suppressing lung inflammation. WT C57BL/6 mice were subcutaneously (s.c.) injected with either vehicle or RTX; the latter leads to denervation of both vagal and spinal sensory neurons[31] (Figure 3F). As expected, s.c. RTX treatment led to delayed paw withdrawal (enhanced withdrawal latency) in response to heat stimulation, indicating loss of noxious sensation (Figure 3G). Strikingly, mice chemically denervated of all sensory neurons, when compared to control mice, had increased peribronchial and perivascular inflammatory infiltrates (Figure 3H), goblet cell hyperplasia, and mucous production (Figure 3I). Further, the frequencies of ILC2s (Figure 3J) and eosinophils (Figure 3K) in the RTX-treated mice were significantly elevated as compared to vehicle-treated control mice. Additionally, transcriptomic analysis of lung tissue revealed upregulation of allergic inflammation-related genes (Figure S2A) and overrepresentation analysis of KEGG pathway revealed an enrichment of asthma- and inflammation-related pathways in the RTX-treated mice as compared to controls (Figure S2B).

We next investigated whether $TRPV1^+$ sensory neurons, arising specifically from the VG, could regulate lung inflammation. To test this possibility, we performed intraganglionic (i.g.) injection of RTX or vehicle control to induce selective loss of sensory neurons from the VG (Figure 3L and S2C). Indeed, i.g. administration of RTX resulted in selective suppression of *Trpv1* expression in the VG, while expression within DRG remained unchanged (Figure S2D–E). Further, chemical denervation of VG-specific sensory neurons did not affect paw withdrawal latency by the hot plate test (Figure 3M). However, denervation of VG-specific sensory neurons significantly affected *Alternaria alternata*-induced lung inflammation, which was evident from increased levels of peribronchial and perivascular inflammatory infiltrates (Figure 3N), goblet cell hyperplasia, and mucous production (Figure 3O) as well as increased frequencies of ILC2s (Figure 3P) and eosinophils (Figure 3Q) in the i.g. RTX-treated mice compared to controls.

We next tested the contribution of spinal sensory neurons from the DRG in regulating lung inflammation. RTX or vehicle was administered intrathecally (i.t.), (Figure S2F) to selectively impair spinal DRG sensory neurons.[31] Indeed, i.t. RTX injection resulted in increased paw withdrawal latency to heat, indicating loss of sensation (Figure S2G). Impairment of DRG sensory neurons did not significantly alter the pathophysiology of *Alternaria alternata*-induced lung inflammation as histopathological analysis revealed no differences in the levels of peribronchial and perivascular inflammatory infiltrates (Figure S2H), goblet cell hyperplasia, and mucous production (Figure S2I) or in the frequencies of ILC2s (Figure S2J) and eosinophils (Figure S2K) between i.t. RTX- and vehicle-treated

control mice. Transcriptomic analysis revealed very few differentially expressed genes (Figure S2L) and KEGG pathway overrepresentation analysis found no specific pathway enrichment induced by i.t. RTX treatment (Figure S2M). Collectively, these findings demonstrate that vagal sensory neurons critically suppress allergic lung inflammation.

Sensory neuron-intrinsic *Jak1* regulates lung inflammation and levels of neuropeptides

Sensory neurons from the DRG express *Jak1* to mediate critical functions such as itch.[10] However, whether *Jak1* is expressed in the VG has not been well addressed. Thus, we reanalyzed scRNA-seq datasets from the VG[28] and found that the majority of $Na_v1.8^+$ sensory neurons co-express *Jak1* (Figures 4A–B). We next hypothesized that *Jak1* expression within vagal sensory neurons may be required for immune homeostasis in the lung. To test this, we employed mice that conditionally lack *Jak1* in $Na_v1.8^+$ neurons (*Jak1*$^{\Delta neuron}$ mice; *Scn10a*^{Cre}:*Jak1*^{flox}) (Figure 4C). Following allergen challenge in the airway, we found that all parameters of inflammation were significantly enhanced in *Jak1*$^{\Delta neuron}$ mice compared to controls, including histopathologic features of lung inflammation (Figures 4D–E) and frequencies of ILC2s (Figure 4F) and eosinophils (Figure 4G). These findings indicate that JAK1 signaling in $Na_v1.8^+$ sensory neurons regulates allergic inflammation in the lung.

We previously showed that both JAK1 and upstream IL-4Rα on spinal sensory neurons critically regulate itch in the setting of skin inflammation.[10] To test whether these pathways exhibit similar overlapping neural functions in the airway, we also subjected *Il4ra*$^{\Delta neuron}$ mice (conditional deletion of *Il4ra* on $Na_v1.8^+$ sensory neurons; *Scn10a*^{Cre}:*Il4ra*^{flox}) to allergic lung inflammation (Figure S3A). However, we found no effect of *Il4ra* deletion in this setting (Figures S3B–F). Thus, despite the presence of a neuronal IL-4Rα-JAK1 itch axis in the skin, IL-4Rα appears dispensable in lung sensory neurons in regulating allergic lung inflammation. Further, given the striking nature of the lung pathology following conditional deletion of *Jak1* in sensory neurons, we sought to test whether neuronal JAK1 signaling may be relevant across multiple model systems. Thus, we employed an alternative mouse model of allergic lung inflammation induced by the protease allergen papain. Following papain challenge in the airway of *Jak1*$^{\Delta neuron}$ mice (Figure S3G), we observed enhanced histopathologic features of lung inflammation (Figures S3H–I) and increased frequencies of $CD45^+$ immune cells (Figure S3J), ILC2s (Figure S3K), and eosinophils (Figure S3L) compared to control mice.

Although our findings demonstrate that neuron-intrinsic JAK1 signaling is required for homeostasis in the face of allergic lung inflammation, whether this function is impacted by JAK1-selective inhibitors in humans remains unclear. Strikingly, recent phase 1 and 2 clinical trials with multiple inhalational JAK1-selective inhibitors have failed in asthma (NCT03766399, NCT04150341, ACTRN12617001227381). Thus, we hypothesized that inhalational delivery of JAK1-selective inhibitors may display limited efficacy *in vivo* due to its restriction to the airway and thus preferential access to sensory neurons; in contrast, systemic delivery of JAK1-selective inhibitors may yet derive efficacy due to their capacity to potently target the hematopoietic compartment. To test this hypothesis, we compared the efficacy of upadacitinib, a JAK1-selective inhibitor, administered either intranasally

(inhalational) or intraperitoneally (systemic) in the *Alternaria alternata*-induced allergic lung inflammation model (Figure S4A). Although both inhalational and systemic delivery of upadacitinib significantly reduced the number of eosinophils in the lung (Figure S4B), only systemic treatment resulted in suppression of ILC2s (Figure S4C). Further, only systemic delivery of upadacitinib resulted in an overall improvement of lung pathology (Figure S4D), goblet cell hyperplasia, and mucous content (Figures S4E). Collectively, these data suggest that inhalational delivery of JAK1-selective inhibitors may have limited efficacy.

Increasing evidence suggests that sensory neurons release neuropeptides to modulate inflammation at multiple barrier surfaces.[13,16,18,32–34] However, the intracellular mechanisms guiding such neuronal responses remain poorly understood. Although JAK1 has been recently appreciated for its ability to relay sensory signals toward the spinal cord (afferent function), whether JAK1 controls expression of neuropeptides in sensory neurons to modulate neuroinflammation in tissues (efferent function) has not been explored. Thus, we sought to screen the expression of various neuropeptides within the VG using existing scRNA-seq datasets.[28] Indeed, both the jugular ganglia (JG) and nodose ganglia (NG) express the classical neuropeptide *Calca*, which encodes the α form (CGRPα) of the neuropeptide used to identify peptidergic neurons (Figures 4H–I). Recent studies have demonstrated the capacity of CGRPα to suppress ILC2 responses in the lung.[16,18] However, the expression of *Calcb* (the gene encoding CGRPβ) and the function of CGRPβ in the lung remain poorly understood. We also screened other neuropeptide genes, including *Tac1* (the gene encoding Substance P [SP]), *Vip* (the gene encoding vasoactive intestinal peptide [VIP]), and *Nmu* (the gene encoding neuromedin U [NMU]) (Figures 4H–I). To visualize the extent of *Calca* and *Calcb* expression within the VG and DRG, we generated reporter mice by crossing *Calca*^{Cre} and *Calcb*$^{Cre/ERT}$ mice, respectively, to *Rosa26*$^{STOPflox\text{-}tdTomato}$ mice. Strikingly, imaging of these reporter mice revealed widespread expression of both *Calca* and *Calcb* in both the VG and DRG (Figures 4J–K).

The ability of JAK1 to alter cellular programs is largely dependent on downstream phosphorylation of STAT proteins, which enter the nucleus to alter transcription. Indeed, overactivity of STAT6 is strongly associated with allergic inflammatory processes, and *STAT6* GOF was recently reported to be associated with similar atopic syndromes as observed for *JAK1* GOF.[35–40] We sought to examine whether STAT6 is associated with regulation of specific neuropeptide regulatory elements via *in silico* analysis of datasets from MotifMap Predicted Transcription Factor Targets (see Methods). We found that *CALCB* and *TAC1*, but not *CALCA, NMU*, and *VIP*, were predicted transcriptional targets of STAT6 (Figure 4L). Further, analysis of transcription factor DNA-binding motifs revealed a STAT6 DNA-binding motif ~500–2000 bp upstream of *CALCB, TAC1*, and *CALCA,* but not *NMU*, and *VIP*, suggesting that STAT6 may selectively regulate expression of genes that encode CGRP and SP. Thus, we hypothesized that JAK1 may regulate CGRPβ and/or SP.

We next subjected both *Jak1*$^{\Delta neuron}$ and control mice to airway allergen challenge and examined the VG for expression of neuropeptide transcripts (Figure S5A). Strikingly, we found that expression of *Calcb* was decreased within the VG (Figure 4M) of *Jak1*$^{\Delta neuron}$ mice compared to control mice. However, this *Calcb* deficiency was not observed within the DRG (Figure 4N). While no alterations were observed in *Calca* and *Vip* expression

(Figures 4O–P and S5B–C), *Tac1* was reduced in both the VG and DRG of *Jak1*$^{\Delta neuron}$ mice (Figures 4Q–R); *Nmu* was only reduced in the DRG of *Jak1*$^{\Delta neuron}$ mice (Figures S5D–E). In contrast to *Jak1*$^{\Delta neuron}$ mice, *JAK1*^{GOF} mice exhibited increased expression of *Calcb*, but not *Tac1*, in their VG compared to control mice (Figures S5F–H). Taken together, these findings indicate that JAK1 regulates the expression of multiple neuropeptides, including *Calcb*, in the VG. Given these findings, along with our *in silico* analysis predicting *CALCB* as a transcriptional target of STAT6, we hypothesized that CGRPβ may be a key regulatory neuropeptide controlled by JAK1.

In light of our findings that both chemical denervation via i.g. RTX (Figures 3L–Q) and sensory neuron-intrinsic deletion of *Jak1* (Figures 4C–G) results in enhanced allergic lung inflammation, we sought to test whether RTX-mediated denervation of TRPV1^{+} sensory neurons impact CGRPβ expression within the vagus nerve. To test this, we treated *Calcb*-reporter (*Calcb*$^{Cre/ERT}$:*Rosa26*$^{STOPflox\text{-}tdTomato}$) mice with i.g. RTX and performed immunofluorescence imaging of total CGRPβ^{+} neurons (Figure S5I). Strikingly, i.g. RTX-mediated denervation demonstrated a marked reduction of CGRPβ^{+} neurons compared to the vehicle-treated mice (Figure S5J–K)

CGRPβ suppresses ILC2 function and allergic lung inflammation

Given that ILC2s are important drivers of allergic lung inflammation[20,41] and the role of CGRPβ in this context is not well understood, we sought to test whether CGRPβ can directly suppress the function of ILC2s in the lungs. We sort-purified lung ILC2s from WT C57BL/6 mice and stimulated them *in vitro* with the alarmin cytokine IL-33, in combination with either CGRPβ or SP (Figure 5A). Strikingly, we found that CGRPβ potently suppressed IL-33-mediated stimulation of IL-5 and IL-13 production from ILC2s (Figures 5B–C). In contrast, the classical proinflammatory neuropeptide SP had no effect on IL-33-elicited activation of lung ILC2s (Figures 5B–C). Similar to CGRPβ, CGRPα also suppressed ILC2 function (Figures S6A–C), a well-known feature of this isoform.[16,18] However, of these two isoforms, only *Calcb* was found to be differentially regulated in the VG of *Jak1*$^{\Delta neuron}$ mice (Figures 4M–P). Our findings demonstrate that CGRPβ can directly suppress ILC2 function and suggest its potential role in restraining allergic lung inflammation.

Allergic lung inflammation is uniquely dependent on ILC2s in adaptive lymphocyte-deficient *Rag1*$^{-/-}$ mice.[19,41] Thus, to specifically evaluate whether exogenous CGRPβ could suppress ILC2 responses *in vivo* and allergic lung inflammation, we challenged *Rag1*$^{-/-}$ mice with intranasal *Alternaria alternata* and simultaneously treated them with either intranasal CGRPβ or the CGRP receptor antagonist CGRPβ 8–37 (Figure 5D). Strikingly, while *Alternaria alternata*-treated and control vehicle-treated *Rag1*$^{-/-}$ mice developed robust ILC2 (Figure 5E) and eosinophil responses (Figure 5F) in association with lung pathology (Figures 5G–H), CGRPβ-treated mice exhibited attenuated immune cell responses (e.g., eosinophils) and tissue inflammation (Figures 5E–H). Conversely, treatment with the CGRPβ receptor antagonist resulted in aggravated allergic lung inflammation (Figures 5E–H). Consistent with our *in vitro* findings (Figures 5A–C), SP did not suppress allergic lung inflammation (Figures S6D–H). To test whether CGRPβ displayed a suppressive function in the presence of adaptive immunity, we also delivered it to the airways of WT mice

with allergic lung inflammation and observed similar anti-inflammatory effects to those observed in *Rag1*$^{-/-}$ mice (Figures S6I–M). Collectively, these findings indicate that while neuron-intrinsic expression of *Jak1* selectively regulates expression of *Calcb* in the VG (Figure 4M), CGRPβ, in turn, has the capacity to regulate lung inflammation.

Retrograde viral delivery and conditional insertion of human *JAK1* GOF into sensory neurons are protective against allergic lung inflammation

Next, we sought to test whether the delivery of human *JAK1* GOF specifically to lung-innervating neurons would be sufficient to suppress allergic lung inflammation. To test this hypothesis, we introduced retrograde Adeno-Associated Virus (AAV) co-expressing Cre recombinase and the human *JAK1* GOF variant into *Rosa26*$^{\text{STOPflox-tdTomato}}$ mice and subjected them to *Alternaria alternata* allergen challenge in the airway (Figure 6A). We found that most reporter-labeled neurons were housed in the VG and were virtually undetectable in the corresponding thoracic DRG (Figures 6B–C and Videos S1–2). These findings indicate that vagal sensory neurons were infected with AAV and thus harbored the *JAK1* GOF variant. Strikingly, histopathological analysis revealed that mice infected with AAV-Cre/*JAK1*$^{\text{GOF}}$ in the airway exhibited robust suppression of allergic lung inflammation (Figures 6D–E) and reduction in the frequencies of CD45^{+} immune cells (Figure 6F), ILC2s (Figure 6G), and eosinophils (Figure 6H).

Finally, we sought to test whether conditional insertion of the same human *JAK1* GOF variant into sensory neurons would be sufficient to suppress allergic lung inflammation as well. Thus, we crossed sensory neuron-specific *Scn10a*$^{\text{Cre}}$ mice with *Jak1*$^{\text{STOPflox-}JAK1\text{ GOF}}$ (*JAK1*^{GOF}:neuron) mice. These mice are conditionally deficient in murine *Jak1*, but harbor human *JAK1*^{GOF} only within sensory neurons. We then subjected these *JAK1*^{GOF}:neuron mice to *Alternaria alternata* allergen challenge in the airway (Figure 6I). Indeed, similar to retrograde viral delivery of the *JAK1* GOF variant, histopathological analysis exhibited robust suppression of allergic lung inflammation (Figures 6J–K) and reduction in the frequencies of CD45^{+} immune cells (Figure 6L), ILC2s (Figure 6M), and eosinophils (Figure 6N). Strikingly, the levels of CGRPβ protein in the airway bronchiolar lavage fluid (BALF) was significantly increased compared to control mice (Figure 6O). Collectively, these findings demonstrate that JAK1 regulates CGRPβ in sensory neurons and promotes immune homeostasis in the lung.

DISCUSSION

The canonical type 2 cytokines IL-4, IL-5, and IL-13 are universally elevated across both AD (eczema) and asthma.[42] However, studies of targeted monoclonal antibody (mAb)-based therapies strongly suggest that although IL-13 is pathogenic in AD, it is a poor target in asthma.[43–47] Conversely, while IL-5 is a driver of asthma, it has failed as a therapeutic target in AD.[48–51] Taken together, these findings suggest that elevated signaling of the same cytokine pathways may imprint different phenotypes across tissues like the skin and lung. Further, while type 2 cytokines share and employ downstream JAK1 signaling to activate different cellular programs,[52] the mechanisms by which JAK1 activity can result in different allergic phenotypes remain unclear. Strikingly, even *JAK1* variants that are

common in the population are associated with AD and eosinophil enrichment but not asthma (see GWAS-based analysis in Methods).[53] Further, while multiple JAK1-selective inhibitors are FDA approved for AD, none are approved for asthma, and multiple inhalational JAK1-selective inhibitors have failed in clinical trials (NCT03766399, NCT04150341, ACTRN12617001227381). These findings suggest that JAK1 signaling has tissue-specific properties that uniquely impact particular diseases and their associated therapies.

By transposing the human *JAK1* GOF allele into mice, we found that while AD-like disease develops spontaneously, activation of JAK1 in vagal sensory neurons confers resistance to allergic lung inflammation. Although patients with *JAK1*^{GOF} spontaneously develop asthma,[11,12] this phenotype was not observed in our *JAK1*^{GOF} mice. We hypothesize that this difference may be due to limited exposure to environmental allergens in laboratory animals. Indeed, protease allergens such as house dust mite can directly stimulate sensory neurons to induce the release of neuropeptides.[54,55] Indeed, only upon challenge with the allergen *Alternaria alternata*, did we observe unique susceptibility to allergic lung inflammation in *JAK1*^{GOF} mice. These findings suggest that, independent of immune hypersensitivity, allergens may disrupt neuroimmune circuits to promote inflammation.

While JAK1 activation in lymphocytes is broadly proinflammatory, our findings suggest that JAK1 activation within the sensory nervous system serves a previously unrecognized immunoregulatory role. This observation may explain why JAK1-selective inhibitors, while highly successful in AD, have not advanced to treatment in asthma.[1] Our findings highlight the need to better understand the cell-specific mechanisms by which cytokines imprint distinct JAK-STAT programs and pathology across different organ systems.

Employing a variety of different chemical, genetic, and viral neuronal manipulation approaches, we found that sensory neuron-intrinsic expression of murine *Jak1* or exogenous human *JAK1*^{GOF} is required to protect against allergen-induced lung inflammation. Further, we found that vagal sensory nerves are the key drivers of this homeostatic mechanism in the airway. By screening various neuropeptides associated with neuroinflammation, we find that JAK1 regulates *Calcb* expression in the VG, and CGRPβ directly suppresses lung inflammation. While recent studies have shown that a number of neuropeptides including NMU, SP, and VIP have proinflammatory functions in the airway,[56–58] CGRPα has demonstrated anti-inflammatory properties.[14,16–18] However, the role of CGRPβ is less understood. Thus, our findings highlight a previously unrecognized and selective role for the CGRPβ isoform in suppressing allergic lung inflammation. Future exploration into the differences between CGRPα and CGRPβ isoforms across tissues may yield deeper insights into barrier immunity and inflammation.

Understanding how various neuropeptides regulate inflammation in the skin, lung, and gut is a major emerging field of neuroimmunology.[13,16,18,32–34] However, the cytokine signals that drive specific neuropeptide programs within these neuroimmune circuits remain poorly understood. The mechanisms by which JAK1 influences the transcription and release of CGRPβ remain unknown. Based on our *in silico* analyses, we suspect that downstream phosphorylation of STAT6 is likely a key mechanism that drives *Calcb* transcription. However, we also speculate that JAK1 may regulate the release of preformed CGRPβ

from the synaptic vesicle in the axon terminal. Thus, JAK1 may have multiple functions within sensory neurons that are both STAT6-independent (CGRPβ protein release) and -dependent (*Calcb* transcription). Future studies aimed at understanding these pathways may reveal functions of JAK1 that are specific to sensory neurons and likely not observed in lymphocytes. Although our study reveals a mechanism by which sensory neurons employ JAK1 as a putative cytokine 'sensor,' discovery and characterization of additional JAK-STAT variants may reveal a highly dynamic landscape by which sensory neurons sense, process, and modulate inflammatory signals in tissues.

Sensory nerves consist of a highly sophisticated system that innervates virtually every organ in the body, including secondary lymphoid organs.[59,60] Although traditionally thought to be only sensory in function, sensory neurons have been found in recent studies to promote barrier immunity to pathogens, regulate metabolism, and even contribute to cancer immunosurveillance.[32,61–65] Thus, our observation that they suppress lung inflammation further underscores an emerging paradigm in which the sensory nervous system may regulate a variety of processes across the organism. Taken together, sensory neuromodulation may soon represent a therapeutic approach to treat a variety of inflammatory, infectious, metabolic, and even malignant disorders.

Limitations of the study

Although we identified a critical link between JAK1 within vagal sensory neurons and its ability to regulate *Calcb* and allergic lung inflammation, our study has limitations. First, the precise mechanisms by which neuron-intrinsic JAK1 modulates transcription, synthesis, and/or release of *Calcb*/CGRPβ remain unknown. Second, the neurons that express *JAK1* within the human VG remain unknown. Third, whether inhibition of human vagal neuron-associated JAK1 alters neuropeptide expression has not been explored. Future studies in primary or iPSC-derived human vagal sensory neurons will be required to understand how our findings translate to human biology.

STAR METHODS

RESOURCE AVAILABILITY

Lead contact—Further information and requests for resources and reagents should be directed to and will be fulfilled by the lead contact, Brian S. Kim (itchdoctor@mountsinai.org).

Materials availability—*JAK1* GOF mice will be made available upon request.

Data and code availability—No original codes were generated in this study.

Accession number is listed in the key resources table to account for all high throughput sequencing data.

EXPERIMENTAL MODEL AND STUDY PARTICIPANT DETAILS

Human study participants—Human study participants study was approved by the institutional review board of the University of British Columbia under protocol number

H15–00641. Patients with *JAK1* GOF variants have been previously described in Del Bel et al.[11] Diagnosis of AD and asthma followed guidelines of the European and North American consensus report[66] and the Global Initiative for Asthma (https://ginasthma.org), respectively. Eczema Area and Severity Index (EASI) was used to score AD severity based on methodology described in Leshem et al.[67] Written informed consent was obtained from parents as study participants were minors at the time of consent.

Animal studies—C57BL/6 wild-type (WT), *Rag1*$^{-/-}$, and *Rosa26*$^{\text{STOPflox-tdTomato}}$ mice were purchased from Jackson Laboratory. Human *JAK1* GOF (*JAK1*$^{\text{GOF}}$) mice and *Jak1*$^{\text{STOPflox-}JAK1\text{ GOF}}$ mice were generated through Cyagen Biosciences, Inc. Schematic of the targeting strategy used to introduce the germline human *JAK1* GOF mutation into the murine *Jak1* locus is outlined in Figure 1H. *Scn10a*$^{\text{Cre}}$ mice were provided by Dr. Rohini Kuner (Heidelberg University, Heidelberg, Germany). *Jak1*$^{\text{flox}}$ mice were purchased from Nanjing Biomedical Research Institute of Nanjing University. *Il4ra*$^{\text{flox}}$ mice were generated by Dr. Frank Brombacher (International Center for Genetic Engineering and Biotechnology, Cape Town, South Africa). *Trpv1*$^{\text{Cre}}$:*Rosa26*$^{\text{STOPflox-tdTomato}}$, *Calca*$^{\text{Cre}}$:*Rosa26*$^{\text{STOPflox-tdTomato}}$, and *Calcb*$^{\text{Cre/ERT}}$:*Rosa26*$^{\text{STOPflox-tdTomato}}$ mice were provided by Dr. Hongzhen Hu (Icahn School of Medicine at Mount Sinai, New York, USA). *Scn10a*$^{\text{Cre}}$: *Jak1*$^{\text{flox}}$ (*Jak1*$^{\Delta neuron}$) mice were generated by crossing *Scn10a*$^{\text{Cre}}$ mice with *Jak1*$^{\text{flox}}$ mice. *Scn10a*$^{\text{Cre}}$:*Il4ra*$^{\text{flox}}$ (*Il4ra*$^{\Delta neuron}$) mice were generated by crossing *Scn10a*$^{\text{Cre}}$ mice with *Il4ra*$^{\text{flox}}$ mice. *Scn10a*$^{\text{Cre}}$:*Rosa26*$^{\text{STOPflox-tdTomato}}$ mice were generated by crossing *Scn10a*$^{\text{Cre}}$ mice with *Rosa26*$^{\text{STOPflox-tdTomato}}$ mice. *Scn10a*$^{\text{Cre}}$:*Jak1*$^{\text{STOPflox-}JAK1\text{ GOF}}$ (*JAK1*$^{\text{GOF:neuron}}$) mice were generated by crossing *Scn10a*$^{\text{Cre}}$ mice with *Jak1*$^{\text{STOPflox-}JAK1\text{ GOF}}$ mice. All mice were housed in specific-pathogenfree (SPF) conditions and environmentally controlled animal facilities with a 12-hour light-dark cycle and were given unrestricted access to food and water. All animal protocols and experiments were approved by the Institutional Animal Care and Use Committee (IACUC) of ISMMS, Washington University School of Medicine in St. Louis, and the National Research Institute for Child Health and Development. All mice (8–13 weeks old, male and/or female) were randomly assigned to experimental groups in an age- and gender-matched fashion, and littermates were used whenever possible. All experiments were performed following strict IACUC guidelines.

METHOD DETAILS

Intranasal administration of *Alternaria alternata* extract, papain, neuropeptides, and JAK inhibitor and lung inflammation assessment—Allergic lung inflammation was induced by intranasal administration of *Alternaria alternata* extract (Greer Laboratories, Inc.; 2 μg/dose in 40 μl of sterile phosphate-buffered saline [PBS]) for four consecutive days (Day 0, 1, 2, and 3) or papain (MilliporeSigma, 20 μg/dose in 40 μl of sterile PBS) for three consecutive days (Day 0, 1, and 2). The effect of exogenous neuropeptides was examined following twice daily (Day −1, 0, 1, 2, and 3) intranasal administration of neuropeptide CGRPβ (Cayman Chemical; 1 μg/dose in 40 μl of sterile PBS) or substance P (Tocris, 50 μg/dose in 40 μl of sterile PBS) prior to *Alternaria alternata* administration. Likewise, the effect of JAK1 inhibition was examined following twice daily (Day 0, 1, 2, and 3) intranasal administration of the JAK1 inhibitor,

upadacitinib (MedChemExpress; 2.5 mg/kg in 40 μl of sterile PBS), prior to *Alternaria alternata* administration. Mice were sacrificed on Day 4 (or on Day 3 for papain) for clinical, histologic, and immunologic analysis. Lungs, collected following PBS perfusion, were processed for immune cell analysis by flow cytometry (right lungs) or fixed in 4% paraformaldehyde for histological analysis (left lungs). Histology slides and digital images were created by HistoWiz Inc. (histowiz.com).

Upadacitinib administration—In the *Alternaria alternata*-induced allergic lung model, upadacitinib was administered intranasally (2.5 mg/kg in 40 μl of sterile PBS) or intraperitoneally (5 mg/kg in 200 μl of sterile PBS) twice daily for four consecutive days (Day 0, 1, 2, and 3).

Tamoxifen administration—Tamoxifen (75 mg/kg in 100 μl corn oil) was administered intraperitoneally for 5 consecutive days, and experiments were performed 7 days post last administration.

Construction of Adeno-Associated Virus (AAV) vectors—AAV2-retro-Cre and AAV2-retro-Cre/hJAK1[NM_002227.4]*(A634D) were constructed by VectorBuilder Inc. (https://en.vectorbuilder.com/). AAV vector transduction protocols followed methods previously described by Su et al. [23] with minor modifications. Briefly, AAV (2×10^3 genome copies/ml) was diluted 10-fold in PBS and was administered intranasally (40 ul/mouse) for four consecutive days, and experiments were performed three weeks after the last administration,.

Flow cytometry—Preparation of lung tissue for flow cytometry followed a slightly modified protocol of Moro et al.,[68]. Briefly, three lobes of the right lung were placed into a solution containing 5 ml Hank's Balanced Salt Solution (HBSS), Liberase TM (Roche; 50 μg/ml final concentration), and DNase I (Roche; 1 μg/ml final concentration) in a gentleMACS™ C-tube (Miltenyi Biotec). Lung tissues were homogenized using protocol "37_m_LDK1" on the gentleMACS™ Dissociator with Heaters (Miltenyi Biotec), then passed through a 70-μm cell strainer (Fisher Scientific) into a 50-ml tube. Any remaining tissue was manually homogenized on the strainer with the end of a 3-ml syringe plunger. The gentleMACS™ C tube and the strainer were washed with 2% (vol/vol) FBS/PBS. The tissue homogenate was centrifuged at 400g for 5 minutes at 4°C, and after discarding the cleared supernatant, the cell pellets were incubated with 1 ml red blood cell lysing buffer (MilliporeSigma) at room temperature for 1 minute followed by a 2% (vol/vol) FBS/PBS wash. Simultaneously, cervical skin lymph nodes from the same mice were processed by homogenizing manually with the end of a 3-ml syringe plunger on a 100-μm cell strainer (Fisher Scientific) directly into a 50-ml tube. The strainer was washed with 2% (vol/vol) FBS/PBS and centrifuged at 400g for 5 minutes at 4°C.

Both the lung and lymph node cell samples were stained with the Zombie NIR viability dye (Biolegend; 1:500) to exclude dead cells, followed by Fc-receptor blocking and cell-surface staining with specific antibodies (key resources table). ILC2s were defined as live $CD45^+$ $CD90^+$ $CD127^+$ Sca-1^+ KLRG-1^+ cells that were negative for lineage markers CD3, CD4, CD8, CD11b, CD11c, B220 (or CD19), MHC-II, Ly6G, and Siglec F within a gate for

lymphocytes. Eosinophils were defined as live $CD45^+$ Siglec F^+ cells within a gate for granulocytes. $CD4^+$ T cells were defined as live $CD45^+$ $CD3^+$ $CD4^+$ cells negative for B220 (or CD19), within a gate for lymphocytes. The cells were analyzed using a Cytek® Aurora (CYTEK) flow cytometer, and the absolute number of cells in each sample was determined using CountBright™ Absolute Counting Beads (Invitrogen).

Bone marrow (BM) transplantation—Recipient mice were supplied with 200 ml of drinking water containing 5 ml of Sulfatrim antibiotic (Sulfamethoxazole/trimethoprim) added into 200 ml of drinking water for one week starting from the day prior to irradiation (Day −1). At the end of Week 1, recipient mice were irradiated (950 cGy) using the X-RAD 320 (Precision X-Ray). Bone marrow was harvested from the femurs and tibias of donor mice, treated with red blood cell lysis buffer (MilliporeSigma) for two minutes, then passed through a 70-μm cell strainer (Fisher Scientific) into a 15-ml conical tube. The cell strainer and cells were washed with 2% (vol/vol) FBS/PBS. ViaStain™ AOPI staining (Nexcelom Bioscience) was used to determine the number of live cells on a Cellometer Auto 2000 (Nexcelom Bioscience). Each recipient mouse received 1×10^7 live BM cells by intravenous (i.v.) infusion within 24 hours following irradiation. Mice were used in experiments four weeks following BM transplantation.

Targeted ablation of TRPV1-expressing peripheral neurons—Chemical ablation of TRPV1-expressing peripheral neurons was performed using Resiniferatoxin (RTX) according to previously published protocols.[14,31] Systemic ablation of TRPV1-expressing neurons was achieved by daily subcutaneously (s.c.) injection of increasing doses of RTX (Alomone Labs; 30, 70, 100 μg/kg for three consecutive days) or vehicle (100 μl saline) in the flanks of C57BL/6 WT mice. Targeted ablation of TRPV1-expressing neurons in the DRG was achieved with daily intrathecal (i.t.; in the L5-L6 region) injection of RTX (25 ng/mouse for two consecutive days) or vehicle (10 μl saline). RTX-treated mice were allowed to rest for 4–6 weeks before use. For targeted ablation of vagal ganglia (VG), TRPV1-expressing neurons in the VG were ablated based on a previously described protocol.[69] Mice were assessed for heat sensitivity with a hot plate test to confirm the functional loss of TRPV1-expressing DRG neurons.[14,31]

C57BL/6 WT mice were injected with RTX intra-ganglionically (i.g.) into the right VG with RTX (25 ng/mouse) or vehicle (0.5 μl saline) using the Remote Infuse/Withdraw Pump 11 Elite Nanomite Programmable Syringe Pump (Harvard Apparatus). RTX-treated mice were allowed to rest for 4–6 weeks before use, and only the right lobes of the lung were used for analysis.

Fluorescent protein imaging in cleared tissue—Tissue samples containing fluorescent tdTomato protein were cleared as previously described.[70] Thoracic segments of mouse DRG and VG were harvested from experimental mice and fixed in 4% paraformaldehyde. Fixed tissues were washed with PBS, placed directly on slides, and covered with the refractive index matching solution, RIMS (40 g Histodenz [MilliporeSigma], 30 ml Phosphate buffer (0.02 M), 0.1% Tween-20 [MilliporeSigma], 0.01% sodium azide). All images were captured using an upright microscope equipped

for epifluorescence microscopy (Nikon 80i; CoolSnapES camera [Nikon Instruments] or FVMPE-RS [Olympus]).

GWAS (genome-wide association studies)-based analysis—GWAS were performed using data obtained from the publicly available GWAS Catalog (https://www.ebi.ac.uk/gwas/genes/JAK1) database, which includes the common *JAK1* variants and their associated phenotypes.

Predicted STAT6 transcriptional targets—Data, obtained from the MotifMap Predicted Transcription Factor Targets dataset (https://maayanlab.cloud/Harmonizome/gene_set/STAT6/MotifMap+Predicted+Transcription+Factor+Targets), were used for analysis. The linked dataset of STAT6 transcriptional targets was used to search genes of interest (*CALCA, CALCB, TAC1, NMU*, and *VIP* are putative targets).

Isolation, culture, and analysis of lung ILC2s—Lung dissociation was performed as previously described.[68] Briefly, pulmonary PBS perfusion through the heart was performed immediately after euthanasia in order to remove circulating cells from the lung vasculature prior to harvesting the lungs. Lung pairs were minced into small pieces using scissors and were placed directly into a gentleMACS™ C-tube (Miltenyi Biotec) containing 5 mL of 1% BSA in HBSS. The lungs were dissociated using the gentleMACS™ Dissociator programmed to protocol “m_lung-01–02.” Following dissociation, the lungs were incubated with collagenase type 5 (Worthington; 200 U/ml final concentration), DNase I (Worthington; 100 U/ml final concentration), and hyaluronidase type 4 (MilliporeSigma; 15000 U/ml final concentration) in a 37 ºC water bath with 40 shakes/minute for 30 minutes. The lungs were then dissociated for a second time using the gentleMACS™ Dissociator with the protocol “m_lung-01–02”. Next, the lung dissociation mixture was filtered through a 70-μm cell strainer (Fisher Scientific) into a 50-ml conical tube, and any pieces remaining on the strainer were manually homogenized with the end of a 3-ml syringe plunger. The conical tubes containing the mixture were centrifuged at 490g for 5 minutes at 4 °C. The supernatant was discarded, and the cell pellet was resuspended in 21 ml of 2% (vol/vol) FBS/PBS and mixed with 9 ml of 100% Percol™ (GE Healthcare). Then, 5 ml of 70% Percol™ was gently added to the bottom of the tube, and the tubes were centrifuged at 490g for 30 minutes at room temperature. After separation, the intermediate layer was carefully moved into a new tube and washed twice with 2% (vol/vol) FBS/PBS. During every wash cycle, the cells suspended in 2% (vol/vol) FBS/PBS were filtered through a 70-μm cell strainer after resuspension. The samples were then incubated in 800 μL Fc block containing 2% (vol/vol) FBS/PBS for 15 minutes. Following incubations, the samples were washed and then incubated with a biotin-conjugated antibody cocktail including lineage markers for 30 minutes. The samples were then washed and incubated with MicroBeads (Miltenyi Biotec) for 20 minutes. Next, the samples were depleted of lineage-positive cells using an AutoMACS (Miltenyi Biotec), and the negative fraction was collected for fluorescence-activated cell sorting (FACS) using a FACSAria™ III Cell Sorter (BD Biosciences). Sorted lung-derived ILC2s were defined as live, lineage (Lin)$^-$, CD45$^+$, CD127$^+$, Sca-1$^+$, and KLRG1$^+$.

Sort-purified lung ILC2s were placed into a 96-well round-bottom plate (300 cells/well, 200 μl/well) and cultured with recombinant mouse IL-2 (R&D, 10 ng/ml final concentration) and/or recombinant mouse IL-33 (R&D; 50 ng/ml final concentration), Substance P (R&D; 10 ng/ml final concentration), CGRPα (R&D; 10 ng/ml final concentration), and CGRPβ (Cayman Chemicals, 10 ng/ml final concentration) for 72 hours. The final supernatant was collected, and levels of IL-5 and IL-13 were measured by ELISA kits (Invitrogen).

RNA isolation from mouse DRG and JG/NG (VG) and qRT-PCR—Mouse DRG or nodose ganglia (NG)/jugular ganglia (JG) (combined VG) were harvested and homogenized with a bead homogenizer (BioSpec) in lysis buffer RA1 (Macherey-Nagel). Total RNA was extracted with the NucleoSpin RNA isolation kit following manufacturer's protocol. Equal amounts of cDNA were synthesized from total RNA extracts using the iScript cDNA Synthesis kit. Gene expression levels were determined using gene-specific primers (key resources table) and 2X qPCR Universal Green MasterMix (Lamda Biotech) or Power SYBR™ Green PCR Master Mix (Thermo Fisher Scientific). Reactions were cycled using a StepOnePlus™ Real-Time PCR System (Thermo Fisher Scientific) or QuantStudio 6 Flex Real-Time PCR System (Thermo Fisher Scientific) using the manufacturer's protocol. Gene expression was normalized to that measured for *Gapdh*, and relative expression was calculated using the ΔΔCt method.

RNA-seq alignment and quality control—Library preparation and sequencing steps of RNA-seq were performed by GENEWIZ from Azenta Life Sciences (genewiz.com). All samples from all experiments were processed using the same pipeline for compatibility. Quality control was performed using FastQC (v0.11.8). Trim Galore! (v0.6.6) was used to trim the adapter sequences with a quality threshold of 20. The GRCm38 genome assembly from GENCODE release M25 was used as a genome and transcriptome reference. The alignment was performed using STAR aligner (v2.7.5b) [71]. Gene-level read counts were obtained using Salmon (v1.2.1) for all libraries.[72] All samples passed the alignment quality control requirements, with >90% of reads uniquely mapping (>10M uniquely mapped reads for each library) using STAR aligner.

Differential mRNA gene expression and pathway analysis—Differential expression analysis was performed using gene-level read counts and the DESeq2 (v1.34.0) R package.[73] Genes with <5 reads in total across all samples were considered inactive genes. A gene was considered differentially expressed if the adjusted p-value (Benjamini-Hochberg procedure) was <0.05 and the absolute $\log_2$(fold change) was >1. Overrepresentation analysis of differentially expressed genes was performed using the clusterProfiler R package (v4.2.2).[74,75] The gene sets used for functional analysis were obtained from the Molecular Signatures Database (MSigDB).[76–78] The overlaps between the differentially expressed genes and the MSigDB gene sets were tested for statistical significance using Fisher's exact test followed by the multiple test correction using the Benjamini-Hochberg procedure (adjusted p-value <0.05).

Single-cell RNA-seq analysis of the JG/NG (VG)—Normalized scRNA-seq expression data for JG and NG neurons was obtained from a previously published study

on vagal sensory neurons.[28] Cells from these datasets that were annotated as non-neuronal cells were filtered out from downstream analysis. The threshold for determining if a cell is positive for a gene was calculated using the method described by Usoskin et. al.[79] and was performed by calculating the average value of the top three cells with the highest expression for that gene and multiplying by 0.05. The numbers of positive cells for the genes *Trpv1, Scn10a, Jak1, Calca, Calcb, Vip, Nmu,* and *Tac1* were calculated using R (v.4.1.0). The numbers of cells positive for the genes *Scn10a, Jak1, Calca, Calcb, Vip, Nmu,* and *Tac1* were calculated from *Trpv1*$^+$ cells. The number of cells positive for *Jak1, Calca, Calcb, Vip, Nmu*, and *Tac1* were also calculated from *Scn10a*$^+$ cells. For both analyses, a global threshold (using all neuronal cells) was calculated.

QUANTIFICATION AND STATISTICAL ANALYSIS

The data are shown as the mean ± standard deviation (SD), unless otherwise indicated. Data from independent experiments are representative of at least two independent replicates or as pooled data. None of the data were excluded from statistical analyses, unless due to technical errors. Statistical significance was determined using unpaired Student's t-tests with Welch's correction, unless otherwise noted. Statistical evaluations were performed using GraphPad Prism 8.0 software (GraphPad Software). Significance is regarded as: $^{\dagger}p < 0.0001$, $***p < 0.001$, $**p < 0.01$, $*p < 0.05$, and n.s. as not significant.

Supplementary Material

Refer to Web version on PubMed Central for supplementary material.

ACKNOWLEDGEMENTS

We thank all members of the Kim lab for their helpful comments and discussion. We thank Drs. Ivan E. de Araujo and Wenfei Han from the Nash Family Department of Neuroscience at Icahn School of Medicine at Mount Sinai (ISMMS) for sharing their mouse vagal nerve isolation protocol. We thank Dr. Rohini Kuner from Heidelberg University for providing *Scn10a*^{Cre} mice and Dr. Frank Brombacher from International Center for Genetic Engineering and Biotechnology in Cape Town for providing *Il4ra*^{flox} mice. This work is supported by the Allen Discovery Center program, a Paul G. Allen Frontiers Group advised program of the Paul G. Allen Family Foundation, the Doris Duke Charitable Foundation, LEO Pharma, and the National Institute of Arthritis and Musculoskeletal and Skin Diseases (NIAMS) (AR070116, AR077007, AR080392) and the National Institute of Allergy and Infectious Disease (NIAID) (AI167933, AI167047) of the National Institutes of Health (NIH). H.H. is supported by the National Institute of Diabetes and Digestive and Kidney Diseases (NIDDK) (DK103901), NIAMS (AR077183), and the National Institute on Alcohol Abuse and Alcoholism (NIAA) (AA027065) of the NIH. R.B.C. is supported by the NIH (AT012041). A.M.V.H. is supported by NIAMS (AR080219). H.Y. is supported by a Crohn's and Colitis Foundation Research Fellowship Award (award number 937437). A.M.T. is supported by the NIAID (AI007163, AI154912). H.M. is supported by a Grant-in-Aid for Scientific Research (B) (20H01622) as well as the National Center for Child Health and Development (#2022B-11). M.T. is supported by a Japanese Society of Allergology International Scholarship.

This work was supported in part through the Bioinformatics for Next Generation Sequencing (BiNGS) shared resource facility within the Tisch Cancer Institute at the ISMMS. The development of this shared resource is partially supported by the NCI P30 (CA196521) Cancer Center support grant, and the ISMMS Skin Biology and Disease Resource-based Center NIAMS P30 award (AR079200). This work was also supported by the computational resources and staff expertise provided by Scientific Computing at ISMMS; the Office of Research Infrastructure of the NIH (S10OD026880); and the ISMMS Genomics Technology Facility.

2. REFERENCES

1. Philips RL, Wang Y, Cheon H, Kanno Y, Gadina M, Sartorelli V, Horvath CM, Darnell JE, Stark GR, and O'Shea JJ (2022). The JAK-STAT pathway at 30: Much learned, much more to do. Cell 185, 3857–3876. 10.1016/j.cell.2022.09.023. [PubMed: 36240739]
2. Bieber T, Simpson EL, Silverberg JI, Thaçi D, Paul C, Pink AE, Kataoka Y, Chu C-Y, DiBonaventura M, Rojo R, et al. (2021). Abrocitinib versus Placebo or Dupilumab for Atopic Dermatitis. New England Journal of Medicine 384, 1101–1112. 10.1056/NEJMoa2019380. [PubMed: 33761207]
3. Guttman-Yassky E, Teixeira HD, Simpson EL, Papp KA, Pangan AL, Blauvelt A, Thaçi D, Chu C-Y, Hong H.C. h., Katoh N, et al. (2021). Once-daily upadacitinib versus placebo in adolescents and adults with moderate-to-severe atopic dermatitis (Measure Up 1 and Measure Up 2): results from two replicate double-blind, randomised controlled phase 3 trials. The Lancet 397, 2151–2168. 10.1016/S0140-6736(21)00588-2.
4. Reich K, Teixeira HD, de Bruin-Weller M, Bieber T, Soong W, Kabashima K, Werfel T, Zeng J, Huang X, Hu X, et al. (2021). Safety and efficacy of upadacitinib in combination with topical corticosteroids in adolescents and adults with moderate-to-severe atopic dermatitis (AD Up): results from a randomised, double-blind, placebo-controlled, phase 3 trial. The Lancet 397, 2169–2181. 10.1016/S0140-6736(21)00589-4.
5. Reich K, Thyssen JP, Blauvelt A, Eyerich K, Soong W, Rice ZP, Hong HC-H, Katoh N, Valenzuela F, DiBonaventura M, et al. (2022). Efficacy and safety of abrocitinib versus dupilumab in adults with moderate-to-severe atopic dermatitis: a randomised, double-blind, multicentre phase 3 trial. Lancet 400, 273–282. 10.1016/S0140-6736(22)01199-0. [PubMed: 35871814]
6. Simpson EL, Sinclair R, Forman S, Wollenberg A, Aschoff R, Cork M, Bieber T, Thyssen JP, Yosipovitch G, Flohr C, et al. (2020). Efficacy and safety of abrocitinib in adults and adolescents with moderate-to-severe atopic dermatitis (JADE MONO-1): a multicentre, double-blind, randomised, placebo-controlled, phase 3 trial. The Lancet 396, 255–266. 10.1016/S0140-6736(20)30732-7.
7. Ytterberg SR, Bhatt DL, Mikuls TR, Koch GG, Fleischmann R, Rivas JL, Germino R, Menon S, Sun Y, Wang C, et al. (2022). Cardiovascular and Cancer Risk with Tofacitinib in Rheumatoid Arthritis. New England Journal of Medicine 386, 316–326. 10.1056/NEJMoa2109927. [PubMed: 35081280]
8. Schwartz DM, Bonelli M, Gadina M, and O'Shea JJ (2016). Type I/II cytokines, JAKs, and new strategies for treating autoimmune diseases. Nature reviews. Rheumatology 12, 25–36. 10.1038/nrrheum.2015.167. [PubMed: 26633291]
9. Villarino AV, Kanno Y, and O'Shea JJ (2017). Mechanisms and consequences of Jak-STAT signaling in the immune system. Nature immunology 18, 374–384. 10.1038/ni.3691. [PubMed: 28323260]
10. Oetjen LK, Mack MR, Feng J, Whelan TM, Niu H, Guo CJ, Chen S, Trier AM, Xu AZ, Tripathi SV, et al. (2017). Sensory Neurons Co-opt Classical Immune Signaling Pathways to Mediate Chronic Itch. Cell 171, 217–228.e213. 10.1016/j.cell.2017.08.006. [PubMed: 28890086]
11. Del Bel KL, Ragotte RJ, Saferali A, Lee S, Vercauteren SM, Mostafavi SA, Schreiber RA, Prendiville JS, Phang MS, Halparin J, et al. (2017). JAK1 gain-of-function causes an autosomal dominant immune dysregulatory and hypereosinophilic syndrome. The Journal of allergy and clinical immunology 139, 2016–2020.e2015. 10.1016/j.jaci.2016.12.957. [PubMed: 28111307]
12. Gruber CN, Calis JJA, Buta S, Evrony G, Martin JC, Uhl SA, Caron R, Jarchin L, Dunkin D, Phelps R, et al. (2020). Complex Autoinflammatory Syndrome Unveils Fundamental Principles of JAK1 Kinase Transcriptional and Biochemical Function. Immunity 53, 672–684.e611. 10.1016/j.immuni.2020.07.006. [PubMed: 32750333]
13. Talbot S, Abdulnour REE, Burkett PR, Lee S, Cronin SJF, Pascal MA, Laedermann C, Foster SL, Tran JV, Lai N, et al. (2015). Silencing Nociceptor Neurons Reduces Allergic Airway Inflammation. Neuron 87, 341–354. 10.1016/j.neuron.2015.06.007. [PubMed: 26119026]
14. Baral P, Umans BD, Li L, Wallrapp A, Bist M, Kirschbaum T, Wei Y, Zhou Y, Kuchroo VK, Burkett PR, et al. (2018). Nociceptor sensory neurons suppress neutrophil and γδ T cell responses in bacterial lung infections and lethal pneumonia. Nature Medicine 24, 417–426. 10.1038/nm.4501.

15. Rochlitzer S, Veres TZ, Kühne K, Prenzler F, Pilzner C, Knothe S, Winkler C, Lauenstein HD, Willart M, Hammad H, et al. (2011). The neuropeptide calcitonin gene-related peptide affects allergic airway inflammation by modulating dendritic cell function. Clinical and experimental allergy : journal of the British Society for Allergy and Clinical Immunology 41, 1609–1621. 10.1111/j.1365-2222.2011.03822.x. [PubMed: 21752117]

16. Wallrapp A, Burkett PR, Riesenfeld SJ, Kim SJ, Christian E, Abdulnour REE, Thakore PI, Schnell A, Lambden C, Herbst RH, et al. (2019). Calcitonin Gene-Related Peptide Negatively Regulates Alarmin-Driven Type 2 Innate Lymphoid Cell Responses. Immunity 51, 709–723.e706. 10.1016/j.immuni.2019.09.005. [PubMed: 31604686]

17. Dakhama A, Kanehiro A, Mäkelä MJ, Loader JE, Larsen GL, and Gelfand EW (2002). Regulation of airway hyperresponsiveness by calcitonin gene-related peptide in allergen sensitized and challenged mice. American journal of respiratory and critical care medicine 165, 1137–1144. 10.1164/ajrccm.165.8.2109058. [PubMed: 11956058]

18. Nagashima H, Mahlakõiv T, Shih HY, Davis FP, Meylan F, Huang Y, Harrison OJ, Yao C, Mikami Y, Urban JF, et al. (2019). Neuropeptide CGRP Limits Group 2 Innate Lymphoid Cell Responses and Constrains Type 2 Inflammation. Immunity 51, 682–695.e686. 10.1016/j.immuni.2019.06.009. [PubMed: 31353223]

19. Bartemes KR, Iijima K, Kobayashi T, Kephart GM, McKenzie AN, and Kita H. (2012). IL-33–Responsive Lineage − CD25 + CD44 hi Lymphoid Cells Mediate Innate Type 2 Immunity and Allergic Inflammation in the Lungs. The Journal of Immunology 188, 1503–1513. 10.4049/jimmunol.1102832. [PubMed: 22198948]

20. Doherty TA, Khorram N, Chang JE, Kim H-K, Rosenthal P, Croft M, and Broide DH (2012). STAT6 regulates natural helper cell proliferation during lung inflammation initiated by Alternaria. Am J Physiol Lung Cell Mol Physiol 303, 577–588. 10.1152/ajplung.00174.2012.-Asthma.

21. Orimo K, Tamari M, Takeda T, Kubo T, Rückert B, Motomura K, Sugiyama H, Yamada A, Saito K, Arae K, et al. (2022). Direct platelet adhesion potentiates group 2 innate lymphoid cell functions. Allergy: European Journal of Allergy and Clinical Immunology 77, 843–855. 10.1111/all.15057. [PubMed: 34402091]

22. Salo PM, Arbes SJ, Sever M, Jaramillo R, Cohn RD, London SJ, and Zeldin DC (2006). Exposure to Alternaria alternata in US homes is associated with asthma symptoms. Journal of Allergy and Clinical Immunology 118, 892–898. 10.1016/j.jaci.2006.07.037. [PubMed: 17030243]

23. Su Y, Barr J, Jaquish A, Xu J, Verheyden JM, and Sun X. (2022). Identification of lung innervating sensory neurons and their target specificity. American Journal of Physiology - Lung Cellular and Molecular Physiology 322, L50–L63. 10.1152/AJPLUNG.00376.2021. [PubMed: 34755535]

24. Akopian AN, Sivilotti L, and Wood JN (1996). A tetrodotoxin-resistant voltage-gated sodium channel expressed by sensory neurons. Nature 379, 257–262. 10.1038/379257a0. [PubMed: 8538791]

25. Akopian AN, Souslova V, England S, Okuse K, Ogata N, Ure J, Smith A, Kerr BJ, McMahon SB, Boyce S, et al. (1999). The tetrodotoxin-resistant sodium channel SNS has a specialized function in pain pathways. Nature neuroscience 2, 541–548. 10.1038/9195. [PubMed: 10448219]

26. Caterina MJ, Schumacher MA, Tominaga M, Rosen TA, Levine JD, and Julius D. (1997). The capsaicin receptor: a heat-activated ion channel in the pain pathway. Nature 389, 816–824. 10.1038/39807. [PubMed: 9349813]

27. Mazzone SB, and Undem BJ (2016). Vagal Afferent Innervation of the Airways in Health and Disease. Physiological Reviews 96, 975–1024. 10.1152/physrev.00039.2015. [PubMed: 27279650]

28. Kupari J, Häring M, Agirre E, Castelo-Branco G, and Ernfors P. (2019). An Atlas of Vagal Sensory Neurons and Their Molecular Specialization. Cell Reports 27, 2508–2523.e2504. 10.1016/j.celrep.2019.04.096. [PubMed: 31116992]

29. De Vries DJ, and Blumberg PM (1989). Thermoregulatory effects of resiniferatoxin in the mouse: Comparison with capsaicin. Life Sciences 44, 711–715. 10.1016/0024-3205(89)90382-2. [PubMed: 2927241]

30. Szallasi A, and Blumberg PM (1989). Resiniferatoxin, a phorbol-related diterpene, acts as an ultrapotent analog of capsaicin, the irritant constituent in red pepper. Neuroscience 30, 515–520. 10.1016/0306-4522(89)90269-8. [PubMed: 2747924]

31. Lai NY, Musser MA, Pinho-Ribeiro FA, Baral P, Jacobson A, Ma P, Potts DE, Chen Z, Paik D, Soualhi S, et al. (2020). Gut-Innervating Nociceptor Neurons Regulate Peyer's Patch Microfold Cells and SFB Levels to Mediate Salmonella Host Defense. Cell 180, 33–49.e22. 10.1016/j.cell.2019.11.014. [PubMed: 31813624]
32. Chu C, Artis D, and Chiu IM (2020). Neuro-immune Interactions in the Tissues. Immunity 52, 464–474. 10.1016/j.immuni.2020.02.017. [PubMed: 32187517]
33. Chu C, Parkhurst CN, Zhang W, Zhou L, Yano H, Arifuzzaman M, and Artis D. (2021). The ChAT-acetylcholine pathway promotes group 2 innate lymphoid cell responses and anti-helminth immunity. Science Immunology 6, 10.1126/sciimmunol.abe3218.
34. Galle-Treger L, Suzuki Y, Patel N, Sankaranarayanan I, Aron JL, Maazi H, Chen L, and Akbari O. (2016). Nicotinic acetylcholine receptor agonist attenuates ILC2-dependent airway hyperreactivity. Nature Communications 7. 10.1038/ncomms13202.
35. Daniel C, Salvekar A, and Schindler U. (2000). A gain-function mutation in STAT6. Journal of Biological Chemistry 275, 14255–14259. 10.1074/jbc.C000129200. [PubMed: 10747856]
36. Sharma M, Lu HY, Vaseghi-Shanjani M, Del Bel KL, van der Lee R, Richmond PA, Lin S, Dalmann J, Lee JJ, Matthews A, et al. (2022). Human Germline Heterozygous Gain-of-Function STAT6 Variants Cause Severe Allergic Disease 2 Running Title: Human germline STAT6 gain-of-function variants. medRxiv. 10.1101/2022.04.25.22274265.
37. Sharma M, Leung D, Momenilandi M, Jones LCW, Pacillo L, James AE, Murrell JR, Delafontaine S, Maimaris J, Vaseghi-Shanjani M, et al. (2023). Human germline heterozygous gain-of-function STAT6 variants cause severe allergic disease. The Journal of experimental medicine 220. 10.1084/jem.20221755.
38. Takeuchi I, Yanagi K, Takada S, Uchiyama T, Igarashi A, Motomura K, Hayashi Y, Nagano N, Matsuoka R, Sugiyama H, et al. (2023). STAT6 gain-of-function variant exacerbates multiple allergic symptoms. The Journal of allergy and clinical immunology 151, 1402–1409.e1406. 10.1016/j.jaci.2022.12.802. [PubMed: 36538978]
39. Suratannon N, Ittiwut C, Dik WA, Ittiwut R, Meesilpavikkai K, Israsena N, Ingrungruanglert P, Dalm VASH, van Daele PLA, Sanpavat A, et al. (2023). A germline STAT6 gain-of-function variant is associated with early-onset allergies. The Journal of allergy and clinical immunology 151, 565–571.e569. 10.1016/j.jaci.2022.09.028. [PubMed: 36216080]
40. Minskaia E, Maimaris J, Jenkins P, Albuquerque AS, Hong Y, Eleftheriou D, Gilmour KC, Grace R, Moreira F, Grimbacher B, et al. (2023). Autosomal Dominant STAT6 Gain of Function Causes Severe Atopy Associated with Lymphoma. Journal of clinical immunology. 10.1007/s10875-023-01530-7.
41. Halim TYF, Krauß RH, Sun AC, and Takei F. (2012). Lung Natural Helper Cells Are a Critical Source of Th2 Cell-Type Cytokines in Protease Allergen-Induced Airway Inflammation. Immunity 36, 451–463. 10.1016/j.immuni.2011.12.020. [PubMed: 22425247]
42. Akdis CA, Arkwright PD, Brüggen MC, Busse W, Gadina M, Guttman-Yassky E, Kabashima K, Mitamura Y, Vian L, Wu J, and Palomares O. (2020). Type 2 immunity in the skin and lungs. Allergy: European Journal of Allergy and Clinical Immunology 75, 1582–1605. 10.1111/all.14318. [PubMed: 32319104]
43. Guttman-Yassky E, Blauvelt A, Eichenfield LF, Paller AS, Armstrong AW, Drew J, Gopalan R, and Simpson EL (2020). Efficacy and Safety of Lebrikizumab, a High-Affinity Interleukin 13 Inhibitor, in Adults with Moderate to Severe Atopic Dermatitis: A Phase 2b Randomized Clinical Trial. JAMA Dermatology 156, 411–420. 10.1001/jamadermatol.2020.0079. [PubMed: 32101256]
44. Hanania NA, Korenblat P, Chapman KR, Bateman ED, Kopecky P, Paggiaro P, Yokoyama A, Olsson J, Gray S, Holweg CTJ, et al. (2016). Efficacy and safety of lebrikizumab in patients with uncontrolled asthma (LAVOLTA I and LAVOLTA II): replicate, phase 3, randomised, double-blind, placebo-controlled trials. The Lancet Respiratory Medicine 4, 781–796. 10.1016/S2213-2600(16)30265-X. [PubMed: 27616196]
45. Panettieri RA, Sjöbring U, Péterffy AM, Wessman P, Bowen K, Piper E, Colice G, and Brightling CE (2018). Tralokinumab for severe, uncontrolled asthma (STRATOS 1 and STRATOS 2): two randomised, double-blind, placebo-controlled, phase 3 clinical trials. The Lancet Respiratory Medicine 6, 511–525. 10.1016/S2213-2600(18)30184-X. [PubMed: 29792288]

46. Simpson EL, Flohr C, Eichenfield LF, Bieber T, Sofen H, Taïeb A, Owen R, Putnam W, Castro M, DeBusk K, et al. (2018). Efficacy and safety of lebrikizumab (an anti-IL-13 monoclonal antibody) in adults with moderate-to-severe atopic dermatitis inadequately controlled by topical corticosteroids: A randomized, placebo-controlled phase II trial (TREBLE). Journal of the American Academy of Dermatology 78, 863–871.e811. 10.1016/j.jaad.2018.01.017. [PubMed: 29353026]

47. Wollenberg A, Blauvelt A, Guttman-Yassky E, Worm M, Lynde C, Lacour JP, Spelman L, Katoh N, Saeki H, Poulin Y, et al. (2021). Tralokinumab for moderate-to-severe atopic dermatitis: results from two 52-week, randomized, double-blind, multicentre, placebo-controlled phase III trials (ECZTRA 1 and ECZTRA 2)*. British Journal of Dermatology 184, 437–449. 10.1111/bjd.19574. [PubMed: 33000465]

48. Bel EH, Wenzel SE, Thompson PJ, Prazma CM, Keene ON, Yancey SW, Ortega HG, and Pavord ID (2014). Oral Glucocorticoid-Sparing Effect of Mepolizumab in Eosinophilic Asthma. New England Journal of Medicine 371, 1189–1197. 10.1056/nejmoa1403291. [PubMed: 25199060]

49. Kang EG, Narayana PK, Pouliquen IJ, Lopez MC, Ferreira-Cornwell MC, and Getsy JA (2020). Efficacy and safety of mepolizumab administered subcutaneously for moderate to severe atopic dermatitis. Allergy: European Journal of Allergy and Clinical Immunology 75, 950–953. 10.1111/all.14050. [PubMed: 31515809]

50. Oldhoff JM, Darsow U, Werfel T, Katzer K, Wulf A, Laifaoui J, Hijnen DJ, Plötz S, Knol EF, Kapp A, et al. (2005). Anti-IL-5 recombinant humanized monoclonal antibody (Mepolizumab) for the treatment of atopic dermatitis. Allergy: European Journal of Allergy and Clinical Immunology 60, 693–696. 10.1111/j.1398-9995.2005.00791.x. [PubMed: 15813818]

51. Pavord ID, Korn S, Howarth P, Bleecker ER, Buhl R, Keene ON, Ortega H, and Chanez P. (2012). Mepolizumab for severe eosinophilic asthma (DREAM): A multicentre, double-blind, placebo-controlled trial. The Lancet 380, 651–659. 10.1016/S0140-6736(12)60988-X.

52. Morris R, Kershaw NJ, and Babon JJ (2018). The molecular details of cytokine signaling via the JAK/STAT pathway. Protein Science 27, 1984–2009. 10.1002/pro.3519. [PubMed: 30267440]

53. Kichaev G, Bhatia G, Loh P-R, Gazal S, Burch K, Freund MK, Schoech A, Pasaniuc B, and Price AL (2019). Leveraging Polygenic Functional Enrichment to Improve GWAS Power. American journal of human genetics 104, 65–75. 10.1016/j.ajhg.2018.11.008. [PubMed: 30595370]

54. Serhan N, Basso L, Sibilano R, Petitfils C, Meixiong J, Bonnart C, Reber LL, Marichal T, Starkl P, Cenac N, et al. (2019). House dust mites activate nociceptormast cell clusters to drive type 2 skin inflammation. Nature immunology 20, 1435–1443. 10.1038/s41590-019-0493-z. [PubMed: 31591569]

55. Perner C, Flayer CH, Zhu X, Aderhold PA, Dewan ZNA, Voisin T, Camire RB, Chow OA, Chiu IM, and Sokol CL (2020). Substance P Release by Sensory Neurons Triggers Dendritic Cell Migration and Initiates the Type-2 Immune Response to Allergens. Immunity 53, 1063–1077.e1067. 10.1016/j.immuni.2020.10.001. [PubMed: 33098765]

56. Wallrapp A, Riesenfeld SJ, Burkett PR, Abdulnour REE, Nyman J, Dionne D, Hofree M, Cuoco MS, Rodman C, Farouq D, et al. (2017). The neuropeptide NMU amplifies ILC2-driven allergic lung inflammation. Nature 549, 351–356. 10.1038/nature24029. [PubMed: 28902842]

57. Nussbaum JC, Van Dyken SJ, von Moltke J, Cheng LE, Mohapatra A, Molofsky AB, Thornton EE, Krummel MF, Chawla A, Liang H-E, and Locksley RM (2013). Type 2 innate lymphoid cells control eosinophil homeostasis. Nature 502, 245–248. 10.1038/nature12526. [PubMed: 24037376]

58. Wang N, Wang J, Zhang Y, Hu S, Zhang T, Wu Y, Sun X, Zhang T, Yang S, and He L. (2022). Substance P-induced lung inflammation in mice is mast cell dependent. Clinical and experimental allergy : journal of the British Society for Allergy and Clinical Immunology 52, 46–58. 10.1111/cea.13902. [PubMed: 33999474]

59. Huang S, Ziegler CGK, Austin J, Mannoun N, Vukovic M, Ordovas-Montanes J, Shalek AK, and von Andrian UH (2021). Lymph nodes are innervated by a unique population of sensory neurons with immunomodulatory potential. Cell 184, 441–459.e425. 10.1016/j.cell.2020.11.028. [PubMed: 33333021]

60. Rosas-Ballina M, Olofsson PS, Ochani M, Valdés-Ferrer SI, Levine YA, Reardon C, Tusche MW, Pavlov VA, Andersson U, Chavan S, et al. (2011). Acetylcholine-synthesizing T cells relay neural

signals in a vagus nerve circuit. Science (New York, N.Y.) 334, 98–101. 10.1126/science.1209985. [PubMed: 21921156]

61. Balood M, Ahmadi M, Eichwald T, Ahmadi A, Majdoubi A, Roversi K, Roversi K, Lucido CT, Restaino AC, Huang S, et al. (2022). Nociceptor neurons affect cancer immunosurveillance. Nature 611, 405–412. 10.1038/s41586-022-05374-w. [PubMed: 36323780]
62. Cohen JA, Edwards TN, Liu AW, Hirai T, Jones MR, Wu J, Li Y, Zhang S, Ho J, Davis BM, et al. (2019). Cutaneous TRPV1+ Neurons Trigger Protective Innate Type 17 Anticipatory Immunity. Cell 178, 919–932.e914. 10.1016/j.cell.2019.06.022. [PubMed: 31353219]
63. Huh JR, and Veiga-Fernandes H. (2020). Neuroimmune circuits in inter-organ communication. Nature Reviews Immunology. Nature Research 20, 217–228. 10.1038/s41577-019-0247-z.
64. Kashem SW, Riedl MS, Yao C, Honda CN, Vulchanova L, and Kaplan DH (2015). Nociceptive Sensory Fibers Drive Interleukin-23 Production from CD301b+ Dermal Dendritic Cells and Drive Protective Cutaneous Immunity. Immunity 43, 515–526. 10.1016/j.immuni.2015.08.016. [PubMed: 26377898]
65. Wang Y, Leung VH, Zhang Y, Nudell VS, Loud M, Servin-Vences MR, Yang D, Wang K, Moya-Garzon MD, Li VL, et al. (2022). The role of somatosensory innervation of adipose tissues. Nature 609, 569–574. 10.1038/s41586-022-05137-7. [PubMed: 36045288]
66. Akdis CA, Akdis M, Bieber T, Bindslev-Jensen C, Boguniewicz M, Eigenmann P, Hamid Q, Kapp A, Leung DYM, Lipozencic J, et al. (2006). Diagnosis and treatment of atopic dermatitis in children and adults: European Academy of Allergology and Clinical Immunology/American Academy of Allergy, Asthma and Immunology/PRACTALL Consensus Report. The Journal of allergy and clinical immunology 118, 152–169. 10.1016/j.jaci.2006.03.045. [PubMed: 16815151]
67. Leshem YA, Hajar T, Hanifin JM, and Simpson EL (2015). What the Eczema Area and Severity Index score tells us about the severity of atopic dermatitis: an interpretability study. The British journal of dermatology 172, 1353–1357. 10.1111/bjd.13662. [PubMed: 25580670]
68. Moro K, Ealey KN, Kabata H, and Koyasu S. (2015). Isolation and analysis of group 2 innate lymphoid cells in mice. Nature Protocols 10, 792–806. 10.1038/nprot.2015.047. [PubMed: 25927389]
69. Han W, and de Araujo IE (2021). Dissection and surgical approaches to the mouse jugular-nodose ganglia. STAR protocols 2, 100474–100474. 10.1016/j.xpro.2021.100474.
70. Yang B, Treweek JB, Kulkarni RP, Deverman BE, Chen CK, Lubeck E, Shah S, Cai L, and Gradinaru V. (2014). Single-cell phenotyping within transparent intact tissue through whole-body clearing. Cell 158, 945–958. 10.1016/j.cell.2014.07.017. [PubMed: 25088144]
71. Dobin A, Davis CA, Schlesinger F, Drenkow J, Zaleski C, Jha S, Batut P, Chaisson M, and Gingeras TR (2013). STAR: ultrafast universal RNA-seq aligner. Bioinformatics (Oxford, England) 29, 15–21. 10.1093/bioinformatics/bts635. [PubMed: 23104886]
72. Patro R, Duggal G, Love MI, Irizarry RA, and Kingsford C. (2017). Salmon provides fast and bias-aware quantification of transcript expression. Nature methods 14, 417–419. 10.1038/nmeth.4197. [PubMed: 28263959]
73. Love MI, Huber W, and Anders S. (2014). Moderated estimation of fold change and dispersion for RNA-seq data with DESeq2. Genome biology 15, 550–550. 10.1186/s13059-014-0550-8. [PubMed: 25516281]
74. Wu T, Hu E, Xu S, Chen M, Guo P, Dai Z, Feng T, Zhou L, Tang W, Zhan L, et al. (2021). clusterProfiler 4.0: A universal enrichment tool for interpreting omics data. Innovation (Cambridge (Mass.)) 2, 100141–100141. 10.1016/j.xinn.2021.100141.
75. Yu G, Wang L-G, Han Y, and He Q-Y (2012). clusterProfiler: an R Package for Comparing Biological Themes Among Gene Clusters. OMICS: A Journal of Integrative Biology 16, 284–287. 10.1089/omi.2011.0118. [PubMed: 22455463]
76. Liberzon A, Birger C, Thorvaldsdóttir H, Ghandi M, Mesirov JP, and Tamayo P. (2015). The Molecular Signatures Database (MSigDB) hallmark gene set collection. Cell systems 1, 417–425. 10.1016/j.cels.2015.12.004. [PubMed: 26771021]
77. Liberzon A, Subramanian A, Pinchback R, Thorvaldsdóttir H, Tamayo P, and Mesirov JP (2011). Molecular signatures database (MSigDB) 3.0. Bioinformatics 27, 1739–1740. 10.1093/bioinformatics/btr260. [PubMed: 21546393]

78. Subramanian A, Tamayo P, Mootha VK, Mukherjee S, Ebert BL, Gillette MA, Paulovich A, Pomeroy SL, Golub TR, Lander ES, and Mesirov JP (2005). Gene set enrichment analysis: a knowledge-based approach for interpreting genome-wide expression profiles. Proceedings of the National Academy of Sciences of the United States of America 102, 15545–15550. 10.1073/pnas.0506580102. [PubMed: 16199517]

79. Usoskin D, Furlan A, Islam S, Abdo H, Lönnerberg P, Lou D, Hjerling-Leffler J, Haeggström J, Kharchenko O, Kharchenko PV, et al. (2015). Unbiased classification of sensory neuron types by large-scale single-cell RNA sequencing. Nature neuroscience 18, 145–153. 10.1038/nn.3881. [PubMed: 25420068]

Highlights

- A human germline *JAK1* GOF variant promotes spontaneous skin inflammation in mice
- Vagal sensory neuron expression of *JAK1* GOF promotes immune homeostasis in the lung
- A neuronal JAK1-CGRPβ axis suppresses ILC2 responses and allergic lung inflammation

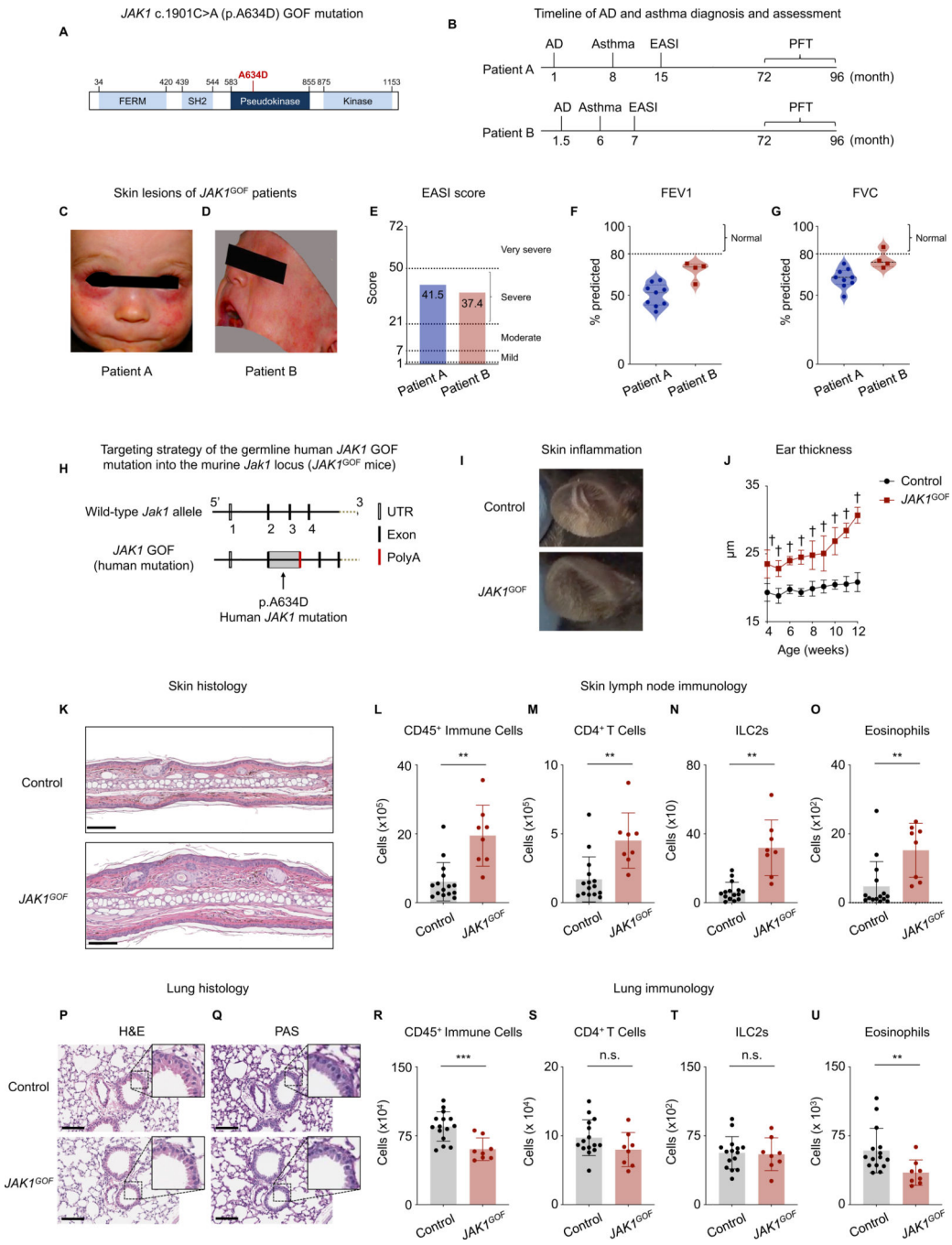

Figure 1. Human germline *JAK1* GOF mutation is associated with AD and asthma in patients and promotes spontaneous AD-like disease in mice

(A) Human *JAK1* c.1901C>A (p.A634D) GOF mutation within the pseudokinase domain.

(B) Timeline of AD and asthma diagnosis, EASI assessment, and PFTs.

(C) Baseline visual image of AD skin lesions from Patient A with a *JAK1* GOF mutation.

(D) Baseline visual image of AD skin lesions from Patient B with a *JAK1* GOF mutation.

(E) Baseline EASI scores from Patient A and Patient B.

(F) Baseline FEV1 of Patient A and Patient B.

(G) Baseline FVC of Patient A and Patient B.

(H) Schematic of the targeting strategy used to introduce the germline human *JAK1* GOF mutation (*JAK1*^{GOF}) into the murine *Jak1* locus.
(I) Representative ear skin images of WT control and *JAK1*^{GOF} mice.
(J) Ear thickness measurements of WT control and *JAK1*^{GOF} mice.
(K) Representative skin histology images (H&E) of WT control and *JAK1*^{GOF} mice. Scale bars indicate 100 μm.
(L-O) Flow cytometry of skin lymph nodes from WT control and *JAK1*^{GOF} mice. Shown are the frequencies of (L) total CD45^{+} immune cells, (M) CD4^{+} T cells, (N) ILC2s, and (O) eosinophils.
(P-Q) Representative lung histology images of WT control and *JAK1*^{GOF} mice, obtained by (P) H&E stain and (Q) PAS stain. Scale bars indicate 200 μm.
(R-U) Flow cytometry of lung tissue from WT control and *JAK1*^{GOF} mice. Shown are the frequencies of (R) total CD45^{+} immune cells, (S) CD4^{+} T cells, (T) ILC2s, and (U) eosinophils.
(J, L-O, R-U) Data were pooled from three independent experiments, n = 8–15 pooled mice per group. $^{\dagger}p < 0.0001$, ***$p < 0.001$, **$p < 0.01$, *$p < 0.05$, and not significant (n.s.) (Unpaired t-test with Welch's correction). Data are represented as mean ± standard deviation (SD).
AD – atopic dermatitis, EASI – eczema area and severity index, FEV1 – forced expiratory volume, FVC – forced vital capacity, GOF – gain-of-function, ILC2s – group 2 innate lymphoid cells, H&E – hematoxylin and eosin, JAK1 – Janus kinase 1, PAS – periodic acid-Schiff, PFT – pulmonary function test, WT – wild-type.
See also Figure S1

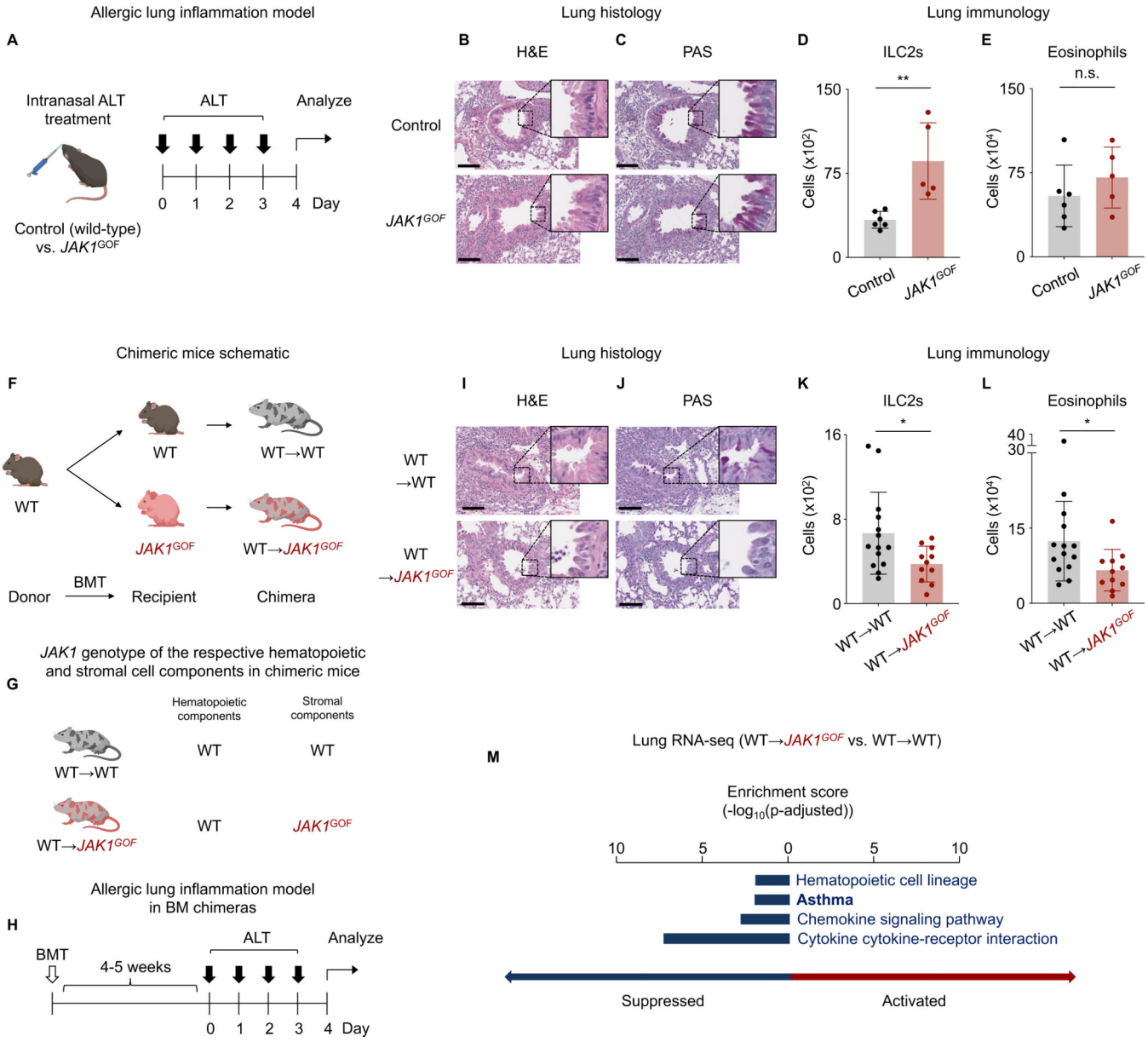

Figure 2. Stroma-intrinsic expression of *JAK1*^{GOF} is protective in allergic lung inflammation

(A) Schematic of the allergic lung inflammation model using the protease allergen *Alternaria alternata* (ALT).

(B-C) Representative lung histology images of WT control and *JAK1*^{GOF} mice challenged with intranasal ALT, obtained by (B) H&E stain and (C) PAS stain.

(D-E) Flow cytometry of lung tissue from WT control and *JAK1*^{GOF} mice challenged with intranasal ALT. Shown are the frequencies of (D) ILC2s and (E) eosinophils. Data were obtained from three independent experiments, n = 5 mice per group.

(F) Schematic of experimental approach used to generate chimeric mice. BM derived from WT mice was transferred into WT control and experimental *JAK1*^{GOF} mice.

(G) *JAK1* genotype of the respective hematopoietic and stromal cell components in chimeric mice (WT→WT and WT→*JAK1*^{GOF}).

(H) Schematic of experimental approach used to generate the allergic lung inflammation model in the BM chimeras.
(I-J) Representative lung histology images of chimeric WT→WT and WT→*JAK1*^{GOF} mice challenged with intranasal ALT, obtained by (I) H&E stain and (J) PAS stain.
(K-L) Flow cytometry of lung tissue from chimeric WT→WT and WT→*JAK1*^{GOF} mice challenged with intranasal ALT. Shown are the frequencies of (K) ILC2s and (L) eosinophils. Data were obtained from three independent experiments, n = 11–14 pooled mice per group.
(M) KEGG pathway overrepresentation analysis of RNA-seq data obtained from the lung tissues of chimeric WT→*JAK1*^{GOF} vs. WT→WT mice (n = 2 mice/group). Overrepresentation analysis used Fisher's exact test to determine the significance of enrichment. All terms shown were identified as the top four significantly suppressed pathways in terms of adjusted p-value (p-adjusted < 0.05, Benjamini-Hochberg procedure).
**p < 0.01, *p < 0.05, and not significant (n.s.) (Unpaired t-test with Welch's correction). Data are represented as mean ± SD. Scale bars indicate 200 μm.
(A, F-G) Figure adapted from an image created with BioRender.com.
ALT- *Alternaria alternata*, BM – Bone marrow, BMT – Bone marrow transplantation.
See also Figure S1

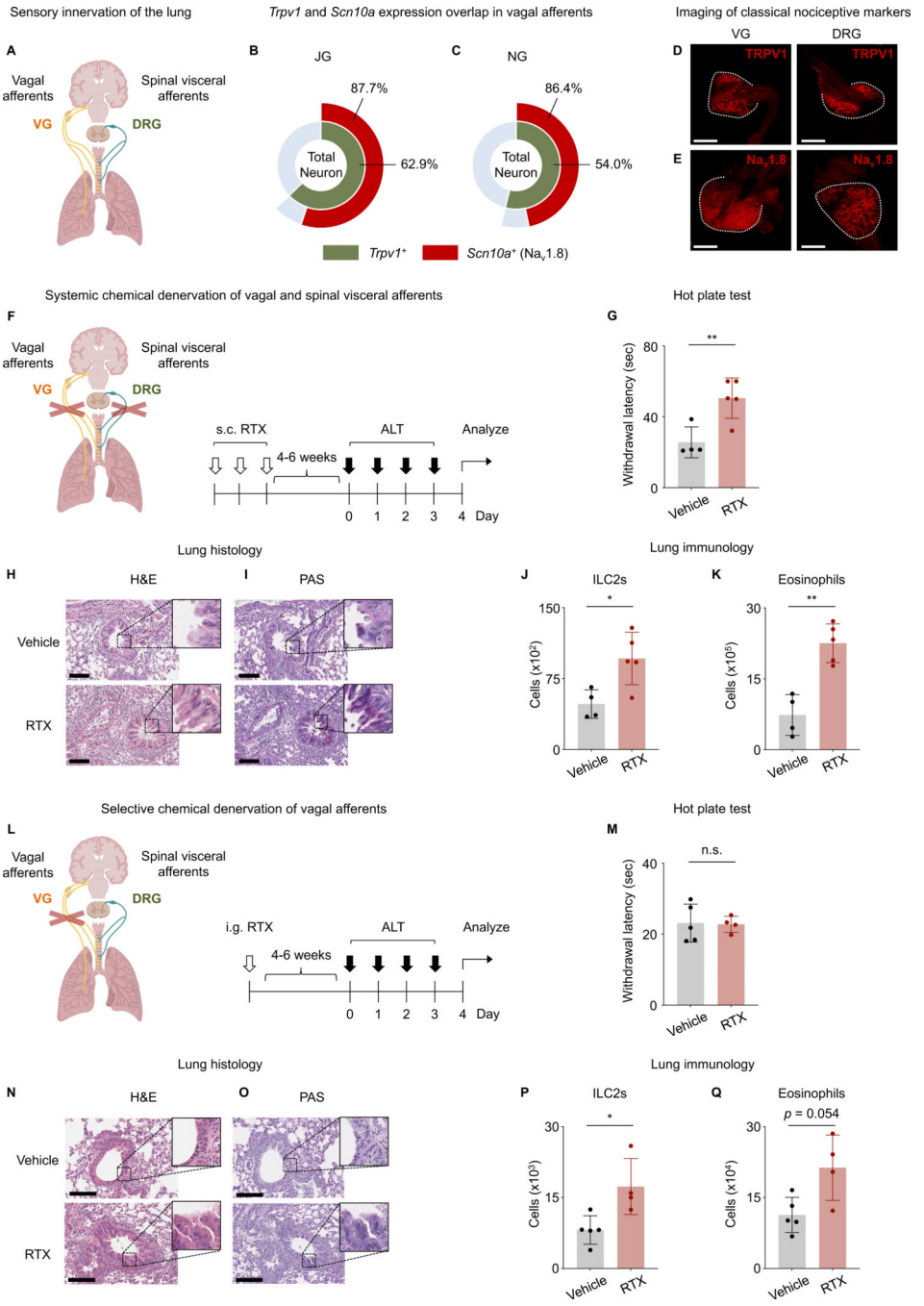

Figure 3. Chemical denervation of TRPV1$^+$ sensory neurons exacerbates allergic lung inflammation

(A) Visual representation of the sensory innervation of the lung arising from the VG and DRG.

(B-C) Expression of *Trpv1* and *Scn10a* (the gene encoding $Na_V1.8$) within the VG, specifically the (B) JG, and (C) NG. *Trpv1* expression is shown as the percentage of total neurons sequenced. *Scn10a* expression is shown as the percentage of *Trpv1*-expressing neurons. The full scRNA-seq dataset is available in Kupari et al.[28]

(D-E) Imaging of classical nociceptive markers (TRPV1 and $Na_v1.8$) in the VG and DRG using *Rosa26*$^{STOPflox\text{-}tdTomato}$ mice crossed with the respective *Trpv1*^{Cre} and *Scn10a*^{Cre} mice. (D) TRPV1 in the VG and DRG, (E) $Na_v1.8$ in the VG and DRG.

(F) Schematic of the allergic lung inflammation model generated following systemic denervation of vagal and spinal visceral afferents.

(G) Withdrawal latency from noxious heat (hot plate test). Mice treated with s.c. vehicle control or RTX were placed on a hot plate set at 50 degrees Celsius, and withdrawal latency was measured as the time until the appearance of paw withdrawal behavior.

(H-I) Representative lung histology images from mice treated with s.c. vehicle control or RTX challenged with intranasal ALT, obtained by (H) H&E stain and (I) PAS stain.

(J-K) Flow cytometry of lung tissue from mice treated with s.c. vehicle control or RTX and challenged with intranasal ALT. Shown are the frequencies of (J) ILC2s and (K) eosinophils. Data were obtained from three independent experiments, n = 4–5 mice per group.

(L) Schematic of the allergic lung inflammation model generated following selective denervation of vagal afferents.

(M) Withdrawal latency from noxious heat (hot plate test). Mice treated with intraganglionic (i.g.) vehicle control or RTX were placed on a hot plate set at 50 degrees Celsius, and withdrawal latency was measured as the time until the appearance of paw withdrawal behavior.

(N-O) Representative lung histology images of mice treated with i.g. vehicle control or RTX challenged with intranasal ALT, obtained by (N) H&E stain and (O) PAS stain.

(P-Q) Flow cytometry of lung tissue from mice treated with i.g. vehicle control or RTX challenged with intranasal ALT. Shown are the frequencies of (P) ILC2s and (Q) eosinophils. Data were obtained from two independent experiments, n = 4–5 mice per group.

$^{**}p < 0.01$, $^{*}p < 0.05$, and not significant (n.s.) (Unpaired t-test with Welch's correction). Data are represented as mean ± SD. Scale bars indicate 200 μm.

(A, F, L) Figure adapted from an image created with BioRender.com.

DRG – dorsal root ganglia, i.g. – intraganglionic, JG – jugular ganglia, NG – nodose ganglia, RTX – resiniferatoxin, s.c. – subcutaneous VG – vagal ganglia

See also Figures S1 and S2

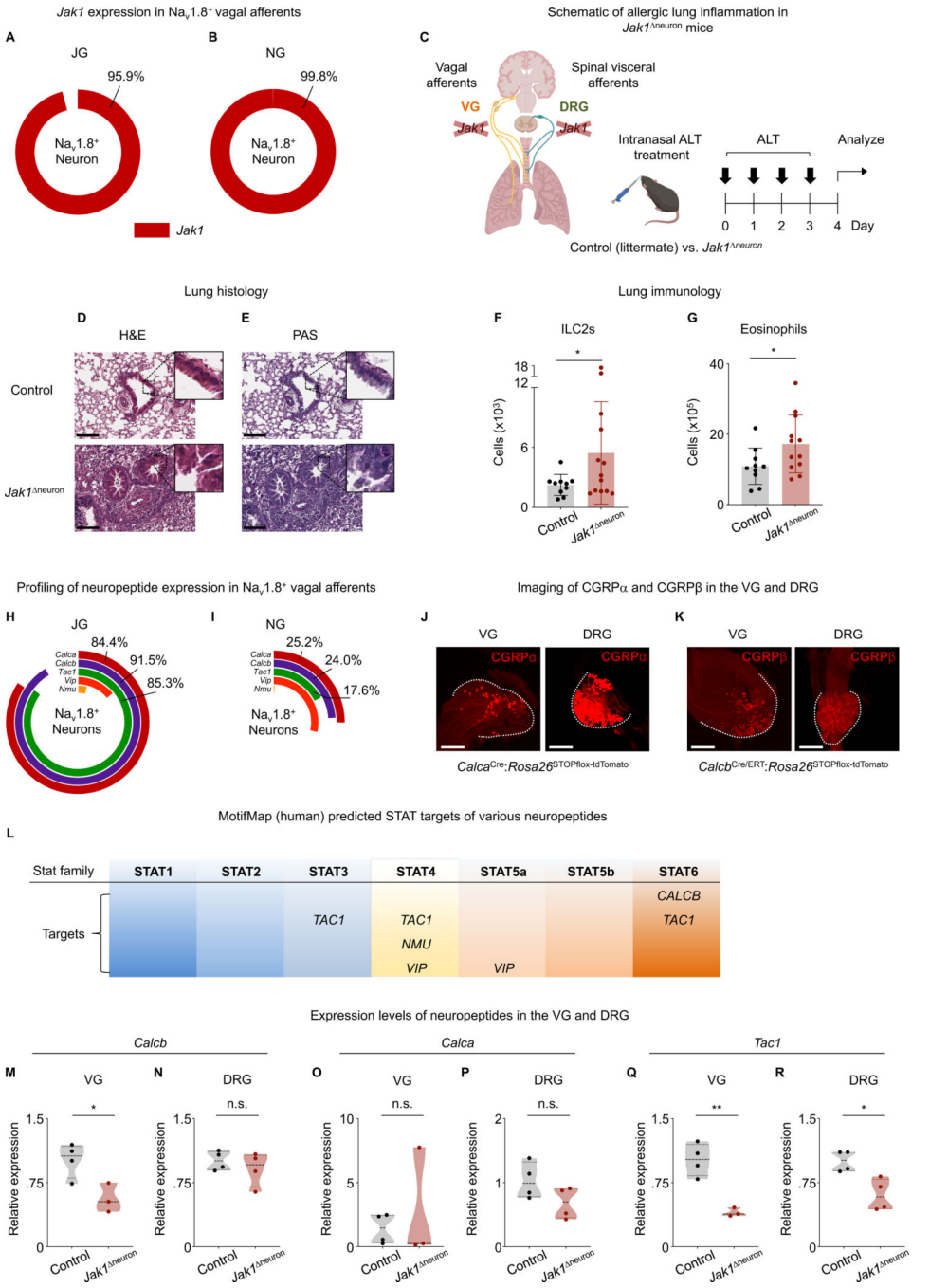

Figure 4. Disruption of sensory neuron-intrinsic *Jak1* exacerbates allergic lung inflammation and alters the expression levels of neuropeptides

(A-B) *Jak1* expression in $Na_V1.8^+$ vagal afferents, (A) JG and (B) NG. Gene expression is shown as the percentage of $Na_V1.8^+$ neurons that express *Jak1*. The full scRNA-seq dataset is available in Kupari et al.[28]

(C) Schematic of the allergic lung inflammation model using littermate control (*Jak1*^{flox}) and experimental *Jak1*$^{\Delta neuron}$ mice.

(D-E) Representative lung histology images of control and *Jak1*$^{\Delta neuron}$ mice challenged with intranasal ALT, obtained by (D) H&E stain and (E) PAS stain.

(F-G) Flow cytometry of lung tissue from control and *Jak1*$^{\Delta neuron}$ mice challenged with intranasal ALT. Shown are the frequencies of (F) ILC2s and (G) eosinophils. Data were obtained from two independent experiments, n = 10–12 pooled mice per group.

(H-I) Profiling of neuropeptide expression in $Na_v1.8^+$ vagal afferents; *Calca*, *Calcb*, *Tac1*, *Vip*, and *Nmu* were evaluated in the (H) JG and (I) NG. Gene expression is shown as the percentage of $Na_v1.8^+$ neurons that express the indicated gene. The full scRNA-seq dataset is available in Kupari et al.[28]

(J-K) Imaging of the classical neuropeptides CGRPα and CGRPβ in the VG and DRG using *Rosa26*$^{STOPflox\text{-}tdTomato}$ mice crossed with *Calca*^{Cre} and *Calcb*$^{Cre/ERT}$ mice, respectively. Shown are (J) CGRPα in the VG and DRG and (K) CGRPβ in the VG and DRG.

(L) MotifMap (human)-predicted neuropeptide targets of STAT family members. Data were analyzed using the MotifMap Predicted Transcription Factor Targets dataset (see Methods).

(M-R) Quantitative PCR (qPCR) of transcripts from the VG and DRG from control and *Jak1*$^{\Delta neuron}$ mice challenged with intranasal ALT. Shown are (M, N) *Calcb*, (O, P) *Calca*, and (Q, R) *Tac1* transcript levels. Data were obtained from two independent experiments, n = 3–4 mice per group.

**p < 0.01, *p < 0.05, and not significant (n.s.) (Unpaired t-test with Welch's correction). Data are represented as mean ± SD. Scale bars indicate 200 μm.

(C) Figure adapted from an image created with BioRender.com.

See also Figures S1 and S3–5

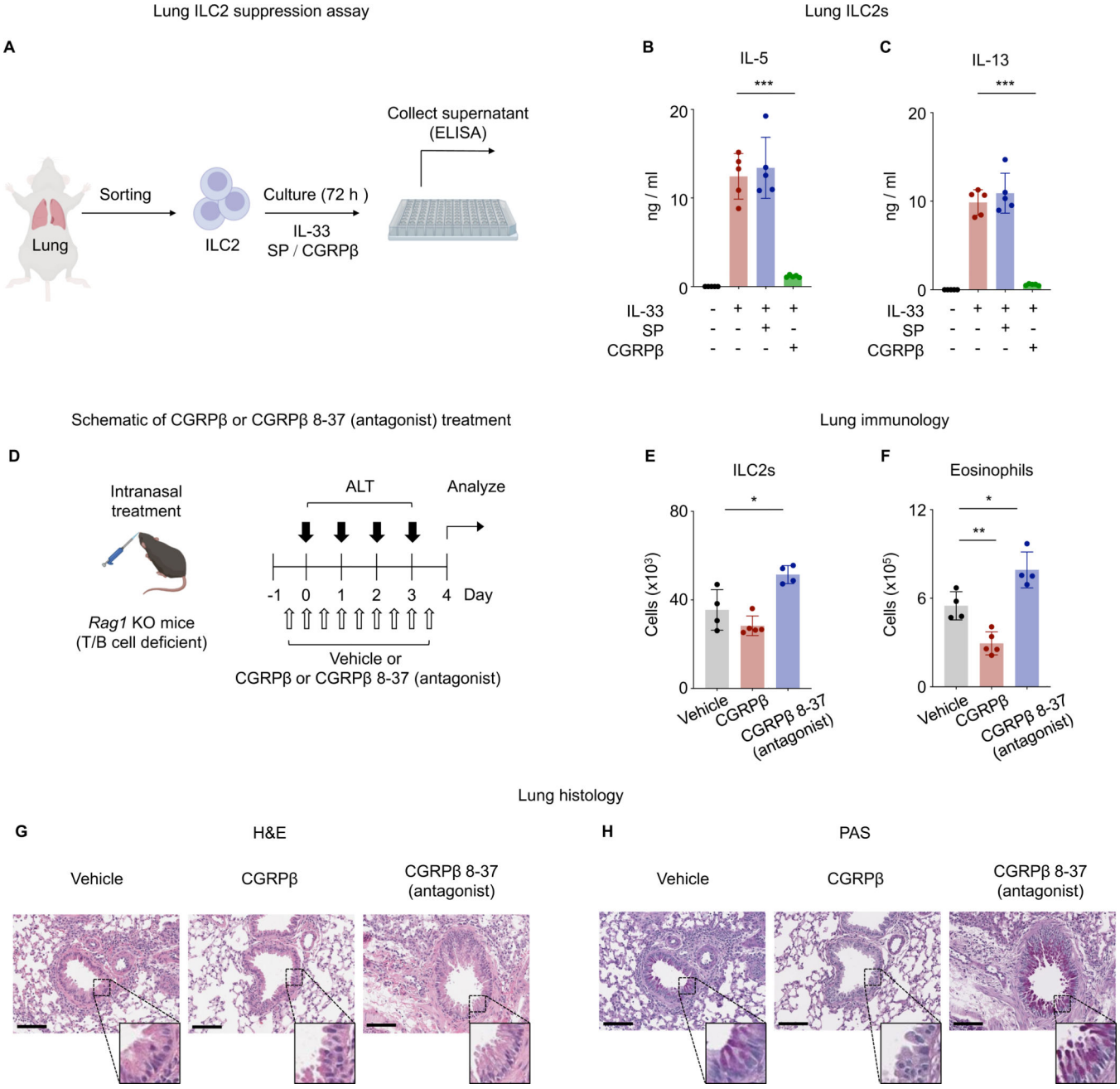

Figure 5. CGRPβ suppresses type 2 cytokine production from lung ILC2s and allergic lung inflammation

(A) Schematic of the lung ILC2 suppression assay.

(B-C) Type 2 cytokine measurement from lung ILC2s stimulated with IL-33, SP, and/or CGRPβ.

Shown are data for (B) IL-5 and (C) IL-13.

(D) Schematic of the induction of allergic lung inflammation in *Rag1*$^{-/-}$ mice.

(E-F) Flow cytometry of lung tissue from *Rag1*$^{-/-}$ mice challenged with intranasal ALT as well as vehicle control or CGRPβ or CGRPβ 8–37. Shown are the frequencies of (E) ILC2s

and (F) eosinophils. Data were obtained from two independent experiments, n = 4–5 mice per group.

(G-H) Representative lung histology images of *Rag1*$^{-/-}$ mice challenged with intranasal ALT as well as vehicle control or CGRPβ or CGRPβ 8–37, obtained by (G) H&E stain and (H) PAS stain.

***p < 0.001, **p < 0.01, *p < 0.05 (Unpaired t-test with Welch's correction). Data are represented as mean ± SD. Scale bars indicate 200 μm.

(A, D) Figure adapted from an image created with BioRender.com.

ELISA – enzyme-linked immunosorbent assay, IL – interleukin, SP – substance P

See also Figures S1 and S6

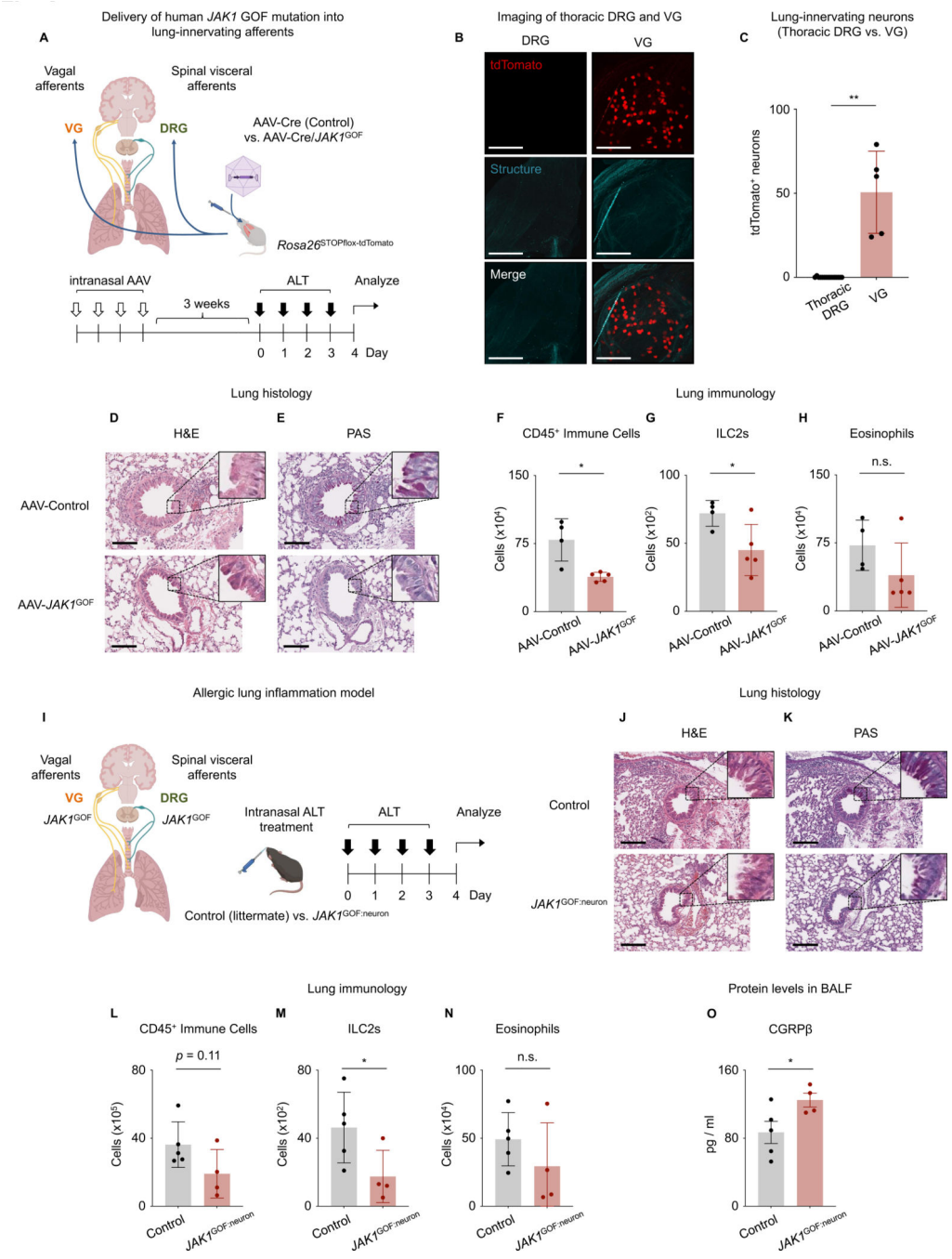

Figure 6. Expression of human *JAK1*^{GOF} in lung sensory neurons suppresses allergic inflammation

(A) Schematic of the allergic lung inflammation model generated by delivery of AAV-Cre (control) or AAV-Cre/*JAK1* ^{GOF} (experimental) into the airways of *Rosa26*$^{STOPflox\text{-}tdTomato}$ mice.

(B) Imaging of tdTomato in the DRG and VG following AAV-assisted gene delivery into lung-innervating sensory neurons. Shown are representative images of DRG and VG from mice treated with AAV-Cre/*JAK1*^{GOF}.

(C) Numbers of tdTomato^{+} neurons in DRG (thoracic segments 4–8) and VG, n = 5 mice per group. Data were analyzed in mice treated with AAV-Cre/*JAK1* GOF.
(D-E) Representative lung histology images of mice challenged with intranasal ALT following AAV-Cre control and AAV-Cre/*JAK1*^{GOF} infection, obtained by (D) H&E stain and (E) PAS stain.
(F-H) Flow cytometry of lung tissue from mice challenged with intranasal ALT following AAV-Cre control and AAV-Cre/*JAK1*^{GOF} infection. Shown are the frequencies of (F) total CD45^{+} immune cells, (G) ILC2s, and (H) eosinophils. Data were obtained from two independent experiments, n = 4–5 mice per group.
(I) Schematic of the allergic lung inflammation model generated by conditional insertion of *JAK1*^{GOF} variant into sensory neurons.
(J-K) Representative lung histology images of mice challenged with intranasal ALT obtained by (J) H&E stain and (K) PAS stain.
(L-N) Flow cytometry of lung tissue from mice challenged with intranasal ALT. Shown are the frequencies of (L) total CD45^{+} immune cells, (M) ILC2s, and (N) eosinophils.
(O) Protein levels of CGRPβ in the bronchoalveolar lavage fluid (BALF). Data were obtained from two independent experiments, n = 4–5 pooled mice per group.
*$p < 0.05$, **$p < 0.01$, and not significant (n.s.) (Unpaired t-test with Welch's correction). Data are represented as mean ± SD. Scale bars indicate 200 μm.
(A, I) Figure adapted from an image created with BioRender.com.
AAV – adeno-associated virus; specifically, AAV2-retro, BALF – Bronchoalveolar lavage fluid
See also Figure S1, Video S1, and S2

KEY RESOURCES TABLE

REAGENT or RESOURCE	SOURCE	IDENTIFIER
Antibodies		
anti-mouse CD16/CD32	Bio X Cell	Cat#: BE0307; RRID: AB_1107647
anti-mouse CD16/32	Biolegend	Cat#: 101302; RRID: AB_312801
anti-mouse CD3	BioLegend	Cat#: 100268; RRID: AB_2876392
anti-mouse CD3	BioLegend	Cat#: 100247; RRID: AB_2572117
anti-mouse CD3e	BioLegend	Cat#: 100304; RRID: AB_312669
anti-mouse CD4	BioLegend	Cat#: 100404; RRID: AB_312689
anti-mouse CD4	BioLegend	Cat#: 100449; RRID: AB_2564587
anti-mouse CD8a	BioLegend	Cat#: 100704; RRID: AB_312743
anti-mouse CD8a	BioLegend	Cat#: 100782; RRID: AB_2819775
anti-mouse/human CD11b	BioLegend	Cat#: 101204; RRID: AB_312787
anti-mouse/human CD11b	BioLegend	Cat#: 101233; RRID: AB_10896949
anti-mouse CD11c	BioLegend	Cat#: 117304; RRID: AB_313773
anti-mouse CD11c	BioLegend	Cat#: 117326; RRID: AB_117326
anti-mouse CD11c	BioLegend	Cat#: 117339; RRID: AB_2562414
anti-mouse CD19	Invitrogen	Cat#: 45-0193-82; RRID: AB_1106999
anti-mouse CD19	Biolegend	Cat#: 115504; RRID: AB_313639
anti-mouse CD45	Invitrogen	Cat#: 58-0451-82; RRID: AB_11218871
anti-mouse CD45	Biolegend	Cat#: 103138; RRID: AB_2563061
anti-mouse CD45R/B220	BioLegend	Cat#: 103275; RRID: AB_2860602
anti-mouse CD90.2	BD Biosciences	Cat#: 740442; RRID: AB_2740169
anti-mouse CD117 (c-Kit)	BioLegend	Cat#: 105838; RRID: AB_2616739
anti-mouse CD117 (c-Kit)	Invitrogen	Cat#: 62-1171-82; RRID: AB_2637141
anti-mouse CD127 (IL-7Ra)	BioLegend	Cat#: 135013; RRID: AB_1937266
anti-mouse CD127 (IL-7Ra)	BioLegend	Cat#: 135035; RRID: AB_2564577
anti-mouse CD127 (IL-7Ra)	BioLegend	Cat#: 135037; RRID: AB_2565269
anti-mouse Siglec-F	BD Bioscience	Cat#: 562757; RRID: AB_2687994
anti-mouse Siglec-F	BioLegend	Cat#: 155506; RRID: AB_2750235
anti-mouse FceRIa	Biolegend	Cat#: 134304; RRID: AB_1626106
anti-mouse I-A/I-E	BioLegend	Cat#: 107622; RRID: AB_493727
anti-mouse/human KLRG1 (MAFA)	BioLegend	Cat#: 138418; RRID: AB_2563015
anti-mouse/human KLRG1 (MAFA)	BioLegend	Cat#: 138419; RRID: AB_2563357
anti-mouse Ly6A/E (Sca-1)	BD Biosciences	Cat#: 749199; RRID: AB_2873577
anti-mouse Ly6A/E (Sca-1)	Biolegend	Cat#: 108112; RRID: AB_313349
anti-mouse Ly-6G	Invitrogen	Cat#: 62-9668-82; RRID: AB_2762763
anti-mouse Ly-6G	BioLegend	Cat#: 127643; RRID: AB_2565971
anti-mouse Ly-6G/Ly-6C (Gr-1)	BioLegend	Cat#: 108404; RRID: AB_313369
Bacterial and virus strains		

REAGENT or RESOURCE	SOURCE	IDENTIFIER
AAV2-retro-Cre	VectorBuilder	Vector ID:VB220605-1075ztp
AAV2-retro-Cre/*JAK1*	VectorBuilder	Vector ID:VB220526-1322bxa
Chemicals, peptides, and recombinant proteins		
Alternaria alternata	GREER	Cat#: NC1620293
β-CGRP (human)	Cayman Chemical	Cat#: 24725
β CGRP 8-37 human	MiliporeSigma	Cat#: SCP0060
Bovine Serum Albumin	MiliporeSigma	Cat#: A9418
Bovine Serum Albumin	MiliporeSigma	Cat#: A9576
CGRP (rat)	R&D	Cat#: 1161
Collagenase Type 5	Worthington Biochemicals	Cat#: LS005282
DNase I	Roche	Cat#: 10104159001
DNase I	Worthington Biochemicals	Cat#: LS002139
Fetal Bovine Serum	MiliporeSigma	Cat#: F4135
Hialuronidase type 4	MiliporeSigma	Cat#: H3384-500MG
Histodenz	MiliporeSigma	Cat#: D2158
Liberase TM	Roche	Cat#: 5401127001
Papain from papaya latex	MiliporeSigma	Cat#: P4762-25MG
Percoll™	GE healthcare	Cat#: 17-0891-2
Quadrol	MiliporeSigma	Cat#: 122262
Resiniferatoxin	Alomone labs	Cat#: R-400
recombinant mouse IL-2	R&D systems	Cat# 402-ML-020/CF
recombinant mouse IL-33	R&D systems	Cat#: 3626-ML-010/CF
Substance P	Tocris	Cat#: 1156
Upadacitinib (ABT-494)	MedChemExpress	Cat#: HY-19569
Critical commercial assays		
Brilliant Violet 421 Streptavidin	Biolegend	Cat#: 405225
CountBrightTM Absolute Counting Beads, for flowcytometry	Invitrogen	Cat#: C36950
Fixation/Permeablization Kit	BD Biosciences	Cat#: 554714
Flexable Viability Dye eFluor™780	Invitrogen	Cat#: 65-0865-18
IL-5 Mouse Uncoated ELISA Kit	Invitrogen	Cat#: 88-7054-88
IL-13 Mouse Uncoated ELISA Kit	Invitrogen	Cat#: 88-7137-22
Mouse CGRP2 ELISA Kit	MyBioSource	Cat#: MBS7241942
Power SYBR™ Green PCR Master Mix	Thermo Fisher Scientific	Cat#: 4367660
Streptavidin Microbeads	Miltenyi Biotec	Cat#: 130-048-101
UltraComp eBeads™ Compensation Beads	Invitrogen	Cat#: 01-2222-42
Viability Dye	Invitrogen	Cat#: 65-0865-14
Zombie NIR™ Fixable Viability Kit	BioLegend	Cat#: 423106
Deposited data		

REAGENT or RESOURCE	SOURCE	IDENTIFIER
Raw and analyzed bulk RNA-seq data	ISMMS BiNGS Core	GEO: GSE220497
Experimental models: Organisms/strains		
C57BL/6J	Jackson Laboratory	Stock No. 000664
C57BL/6J	Sankyo Labo Service Corpration, Inc.	N/A
Calca^{Cre}: *Rosa26*$^{STOPflox\text{-}tdTomato}$	Hongzhen Hu	N/A
Calcb$^{Cre/ERT}$: *Rosa26*$^{STOPflox\text{-}tdTomato}$	Hongzhen Hu	N/A
Calcb$^{Cre/ERT}$: *Rosa26*$^{STOPflox\text{-}tdTomato}$	Brian Kim	N/A
Il4ra^{flox}	Frank Brombacher	N/A
Jak1^{flox}	Nanjing Biomedical Research Institute	N/A
Jak1$^{STOPflox\text{-}JAK1\ GOF}$	Cyagen Biosciences Inc.	N/A
JAK1^{GOF}	Cyagen Biosciences Inc.	N/A
Scn10a^{Cre}	Rohini Kuner	N/A
Scn10a^{Cre}: *Il4ra*^{flox}	Brian Kim	N/A
Scn10a^{Cre}: *Jak1*flox	Brian Kim	N/A
*Scn10a*Cre: *Jak1*$^{STOPflox\text{-}JAK1\ GOF}$	Brian Kim	N/A
*Scn10a*Cre: *Rosa26*$^{STOPflox\text{-}tdTomato}$	Brian Kim	N/A
Trpv1^{Cre}: *Rosa26*$^{STOPflox\text{-}tdTomato}$	Hongzhen Hu	N/A
Rag1 $^{-/-}$	Jackson Laboratory	Stock No. 002216
Rosa26$^{STOPflox\text{-}tdTomato}$	Jackson Laboratory	Stock No. 007909
Oligonucleotides		
Gapdh qRT-PCR primer 1	integrated DNA Technologies	TCAAGAAGGTGGTGAAGCAGG
Gapdh qRT-PCR primer 2	integrated DNA Technologies	TATTATGGGGGTCTGGGATGG
Calca qRT-PCR primer 1	integrated DNA Technologies	GAGGGCTCTAGCTTGGACAG
Calca qRT-PCR primer 2	integrated DNA Technologies	AAGGTGTGAAACTTGTTGAGGT
Calcb qRT-PCR primer 1	integrated DNA Technologies	CTCTCAGCACGATATGGGTCC
Calcb qRT-PCR primer 2	integrated DNA Technologies	GCAAGAGATGTTTTTCCTGGTCG
Nmu qRT-PCR primer 1	integrated DNA Technologies	GAGGGAGCTTTGCCGTATAGT
Nmu qRT-PCR primer 2	integrated DNA Technologies	GATGCACAACAGAGGACACAA
Tac1 qRT-PCR primer 1	integrated DNA Technologies	TTTCTCGTTTCCACTCAACTGTT
Tac1 qRT-PCR primer 2	integrated DNA Technologies	GTCTTCGGGCGATTCTCTGC
Trpv1 qRT-PCR primer 1	Thermo Fisher Scientific	AGCTGCAGCGAGCCATCACCA
Trpv1 qRT-PCR primer 2	Thermo Fisher Scientific	ATCCTTGCCGTCCGGCGTGA
Vip qRT-PCR primer 1	integrated DNA Technologies	AGTGTGCTGTTCTCTCAGTCG
Vip qRT-PCR primer 2	integrated DNA Technologies	GCCATTTTCTGCTAAGGGATTCT
Software and algorithms		
clusterProfiler R package (v4.2.2)	G Yu et. al	https://guangchuangyu.github.io/software/clusterProfiler/
DEGReport R package (v1.30.3)	L Pantano	https://github.com/lpantano/DEGreport

REAGENT or RESOURCE	SOURCE	IDENTIFIER
DESeq2 (v1.34.0) R package	M Love et. al	https://github.com/mikelove/DESeq2
FastQC (v0.11.8)	Babraham Bioinformatics	https://www.bioinformatics.babraham.ac.uk/projects/fastqc/
FlowJo 10	Tree Star	https://www.flowjo.com/
Galore! (v0.6.6)	Babraham Bioinformatics	https://www.bioinformatics.babraham.ac.uk/projects/trim_galore/
Glimma (v2.4.0) R packages	S Su et. al	https://github.com/Shians/Glimma
NIS-Elements	Nikon Instruments	https://www.microscope.healthcare.nikon.com/products/software
plotly R package (v4.9.4.1)	C Sievert et. al	https://plotly.com/r/
Prism 9	GraphPad Software	https://www.graphpad.com/scientificsoftware/prism/
R (v.4.1.0)	R Core Team	https://www.r-project.org/
STAR aligner (v2.7.5b)	A Dobin et. al	https://github.com/alexdobin/STAR
Salmon (v1.2.1)	R Patro et. al	https://combine-lab.github.io/salmon/
Ugent Center for Plant Systems Biology online tool	UCPSB: Bioinformatics & Evolutionary Genomics	https://bioinformatics.psb.ugent.be/webtools/Venn/
Other		
AutoMACS	Miltenyi Biotec	N/A
Bead Homogenizer	BioSpec	Cat#: 112011
Cytek® Aurora	CYTEK	N/A
FACSAria™ III Cell Sorter	BD	N/A
FVMPE-RS	Olympus	N/A
gentleMACS™ Octo Dissociator with Heaters	Miltenyi Biotec	Cat#: 130-096-427
Nikon 80i; CoolSnap ES camera	Nikon Instruments	N/A
QuantStudio 6 Flex Real-Time PCR Systems	Thermo Fisher Scitntific	N/A
Remote Infuse/Withdraw Pump 11 Elite Nanomite Programmable Syringe Pump	Harvard Apparatus	70-4507
StepOnePlus qRT-PCR System	Thermo Fisher Scientific	N/A